Fabrication, Properties and Applications of Gold Nanopillars

11

Dorothea Brüggemann, Bernhard Wolfrum, and Johann P. de Silva

Keywords

Biosensing • Microelectrodes • Nanocylinder • Nanoelectrodes • Nanofabrication • Nanoimprint lithography • Nanomechanical properties • Nanopillar • Nanorod • Plasmonics

Introduction

Nanotechnology has brought forward the design of various gold nanostructures with a vast variety of different nanoarchitectures. The outstanding optical properties of gold nanoparticles and flower or waxberry-like gold nanostructures – a result of surface-plasmon oscillations – have made these nanomaterials very attractive for applications in sensing, diagnostics, or photothermal therapeutics [1, 2]. Lying gold nanorods fabricated via chemical synthesis exhibited excellent properties for optical imaging or plasmonic waveguide applications [3, 4]. Biosensing devices have benefited hugely from the biocompatibility and excellent electronic properties of

D. Brüggemann (✉)
School of Physics and CRANN, Trinity College Dublin, Dublin, Ireland

Department of New Materials and Biosystems, Max Planck Institute for Intelligent Systems, Stuttgart, Germany
e-mail: brueggemann@is.mpg.de

B. Wolfrum
Institute of Bioelectronics (PGI-8/ICS-8), Forschungszentrum Jülich, Jülich, Germany

IV. Institute of Physics, RWTH Aachen University, Aachen, Germany
e-mail: b.wolfrum@fz-juelich.de

J.P. de Silva
School of Physics and CRANN, Trinity College Dublin, Dublin, Ireland
e-mail: j.desilva@physics.org

B. Bhushan et al. (eds.), *Handbook of Nanomaterials Properties*,
DOI 10.1007/978-3-642-31107-9_55,

nanoporous gold and gold nanoflakes as low-impedance electrodes [5–7] or gold microspines for cell recordings and improved cell adhesion [8, 9].

The sensitivity of biosensors and plasmonic devices can be increased with nanostructures of high aspect ratios: this makes vertical gold nanopillars excellent candidates for these applications. To date, nanopillars have already been produced from a large variety of materials, ranging from polymers [10], silicon [11], SiO_2 [12, 13], and GaAs [14] to various metallic nanopillars such as copper [15, 16], platinum [17], nickel [18, 19], and silver [20]. Gold nanopillars in particular have several advantages over other metallic nanopillars: they are chemically inert, biocompatible, and offer various possible surface functionalizations via thiol coupling, for example [21]. Furthermore, gold nanopillars combine excellent optical properties based on surface-plasmon resonance and also outstanding electronic properties. Several methods such as template-assisted synthesis, various microfabrication techniques, and less well-known approaches have been established to fabricate gold nanopillars. The geometry and long-range order of gold nanopillar arrays can be tailored by these different fabrication techniques. However, to date gold nanopillars have only been produced in a research laboratory environment and are not yet commercially available.

In this chapter we present established and novel techniques for the fabrication of gold nanopillars (Template-Assisted Synthesis to Other Fabrication Techniques) and also focus on the prepatterning of these nanostructures (Fabrication of Prepatterned Nanopillars). Furthermore, we shall discuss the versatile material properties of gold nanopillars (Mechanical Stability to Electrochemical Properties) and their potential for various surface modifications (Self-Assembled Monolayer Coatings to Metal Oxide Coatings) and metamaterials (Metamaterials). From these attributes a wide application range for gold nanopillars has evolved, and here we discuss recent applications of gold nanopillars in the fields of biosensing (Biosensing Employing Nanopillar Electrodes) and plasmonic devices (Gold Nanopillars in Plasmonic Devices).

Fabrication Methods

Various fabrication techniques have already been implemented for the fabrication of gold nanopillars. Most commonly, gold is electrochemically deposited onto nanoporous templates with vertical nanochannels. This simple fabrication method yields good reproducibility of gold nanopillars with a versatile range of geometries and aspect ratios combined with low costs [22, 23]. Often gold nanopillars are also produced by focused ion beam (FIB) milling or nanoimprint lithography (NIL). Microfabrication equipment is required for these techniques, which increases the cost of gold nanopillars fabricated by such methods. Conversely, very precise geometries with high reproducibility over a large surface area can be facilitated when microfabrication techniques are used. FIB-machined gold nanopillars especially can be produced with a larger range of diameters and lengths than other common methods (see Table 11.1) [24]. Electron beam lithography can also be employed for the fabrication of gold nanopillars; in this approach a photoresist is

Table 11.1 Range of possible nanopillar geometries for various fabrication methods

Fabrication method	Diameter (nm)	Height (nm)	Features	References
Anodic aluminum oxide template-assisted deposition	15–200	100–8,000	Simple, low-cost method with high reproducibility and large geometry range	[40–43]
Focused ion beam milling	50–8,000	30 to 11,000	Direct pillar fabrication with large geometry range and very high reproducibility, high costs	[28, 62]
Nanoimprint lithography	100–1,100	50–4,000	Coating of polymer casts is common, high costs	[20, 63, 69–71]
Electron beam lithography	50–200	50–285	Combination with metal deposition, good reproducibility, high costs	[25, 45]

prestructured to serve as a mask, and gold is subsequently deposited onto this mask to obtain nanopillars [25, 26]. Despite good reproducibility this method is not widely used due to the high costs that are involved. Two rare fabrication methods, which have only been introduced recently, are the assembly of gold nanoparticles into pillars using a polymer mask [27] and decomposition from an organometallic precursor [28].

Established and novel fabrication methods for gold nanopillars and the resulting geometries are presented in this section. We also focus on prepatterning approaches for the production of localized pillars with long-range order.

Template-Assisted Synthesis

The use of nanoporous template materials for the fabrication of vertical metal nanowires was first established by Possin in 1970 [29], where he used track-etched mica membranes to produce indium, tin, and zinc nanowires of 40 nm diameter and up to 15 μm length. At this stage, the fabrication of gold nanopillars was not yet possible, but other metal, organic, and polymer nanopillars were subsequently produced via template synthesis. In the following years template-assisted nanopillar synthesis has been developed further, and other template materials were introduced [30].

Template Materials

Several template materials may be used in the fabrication of gold nanopillars: the most common templates with cylindrical pores of uniform diameter are anodic aluminum oxide and track-etched polymer membranes. Other template materials with a nanochannel architecture are, for example, glass, silica aerogels, titania, or mesoporous zeolites [22, 31, 32]. The pore diameter and distribution in the respective nanoporous template material determines the resulting pillar geometry and arrangement.

Nanoporous anodic aluminum oxide (AAO) membranes are fabricated from aluminum in a very efficient and low-cost anodization process with polyprotic acids such as oxalic, sulfuric, or phosphoric acid [33]. The self-assembled parallel nanochannels grow perpendicularly to the surface with uniform pore sizes and lengths, which can exceed 100 μm [34]. By adjusting anodization voltage, time, and pH value of the acid, the pore geometries can be controlled accurately. These variations yield pore diameters ranging from only 4 nm up to several hundred nanometers, and pore densities can reach up to 10^{11} pores per cm^2 [31]. Furthermore, AAO membranes are commercially available with a limited number of pore sizes (such as Anopore™ from Whatman or Unikera™ from Synkera Technologies) [22].

Track-etched polymer membranes, also known as nuclear track filters or screen membranes, are fabricated through heavy ion bombardment of polymer sheets such as polycarbonate (PC) or polyester [31]. Subsequently, the ion tracks are chemically etched to transform the damaged area into a hollow nanochannel. Cylindrical and cone-shaped pores can be achieved via this step, which is controlled by the chemical nature of the etchant, KOH or HF, for example, concentration, temperature, or the total etch time [35]. The etch rate of the membrane material and the presence of any surfactants are also important parameters [36]. The ion bombardment results in nanopores that are slightly tilted with respect to the surface of the sheets [22]. Pore diameters between 10 nm and tens of microns may be produced by ion bombardment and track etching, and pore densities up to 10^9 pores per cm^2 are possible [30, 37]. These membranes are also available commercially for a wide range of filtering applications (Nucleopore® from PCI Scientific, Poretics® from Sphaero Q, Cyclopore™ from Whatman, Osmonics from Lenntech, Isopore™ from Millipore) [31].

Microfabricated masks are another template material that can be used for the synthesis of gold nanopillars: the advantage here is that the nanochannel architecture can be adjusted very precisely by controlling the process parameters, thus enabling the fabrication of localized gold nanopillars with long-range order (see section ‘Fabrication of Prepatterned Nanopillars’).

Deposition Techniques

Electrochemical Deposition

Two decades after the first metal nanopillars were produced by Possin et al., the electrochemical deposition of gold nanopillars into nanoporous AAO templates [38] and track-etched membranes [39] was presented by Martin et al. for the first time. To obtain gold nanopillars electrochemically via template synthesis, one side of the nanoporous membranes is coated with a gold film by sputtering or thermal evaporation. This film serves as a cathode in the subsequent electroplating step [22]. After depositing gold the AAO membrane is dissolved (in KOH, for instance), to obtain freestanding gold nanopillars (see Fig. 11.1). In this process the geometry of the nanoporous template determines the dimensions of the resulting nanopillars. The nanopillar length depends on the

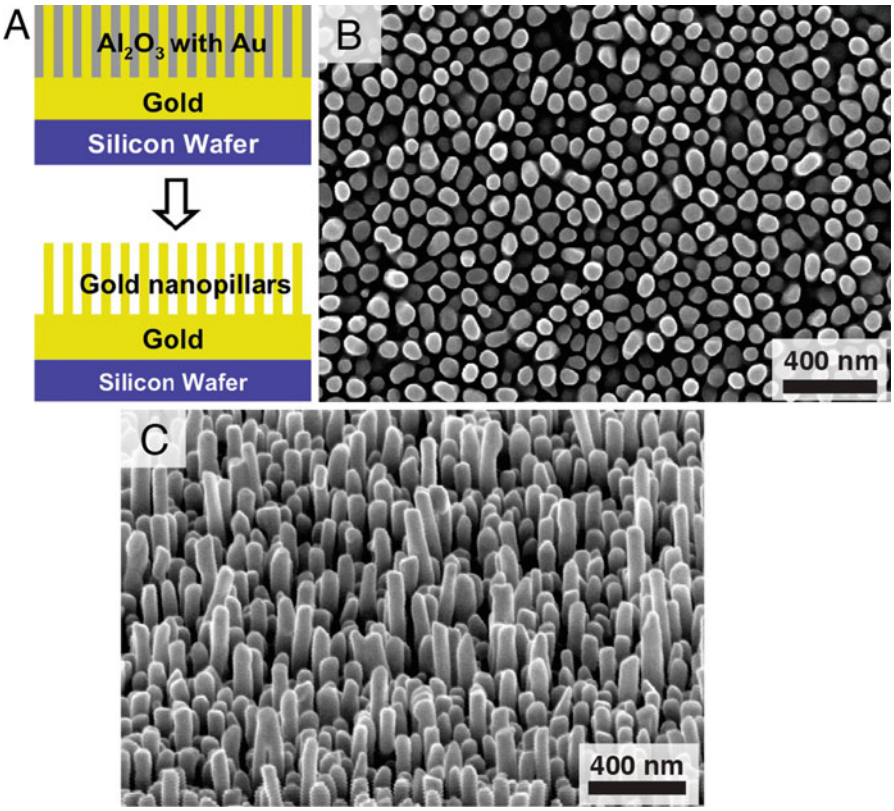

Fig. 11.1 (**A**) Schematic view of gold nanopillars fabricated via electrochemical template synthesis. After gold has been deposited into the nanochannels of an AAO membrane, the template is removed, thus yielding freestanding gold nanopillars (**B**) and (**C**) scanning electron micrograph of gold nanopillars prepared via electrochemical deposition into AAO membranes, in both plan and tilted projections

membrane thickness and can be accurately controlled by the amount of gold deposited, i.e., by varying the deposition time. Tailoring the pillar height enables the fabrication of gold nanostructures with variable aspect ratios (length to diameter), which is important for the optical properties of nanostructured metals [23], for example. Gold nanopillars that are electrodeposited onto AAO membranes have been fabricated with diameters between 15 nm [40] and 200 nm [41] and heights ranging from 100 nm [42] to 8 μm [43] (see Table 11.1).

Martin et al. found that electrochemical deposition of gold into AAO pores yields two different nanostructures depending on the presence of an organocyanide molecular anchor. When an anchor such as (2-cyanoethyl) triethoxysilane is attached to the pore walls, the formation of hollow gold tubules takes place, whereas the absence of any molecular anchors results in the growth

of solid Au nanopillars [38]. This modification of the pore walls with a silane derivative was reported as pore-wall-modified electrodeposition [37].

After 2000 electrodeposition of gold into photoresist masks was presented by Greer et al. [44] and Nagel et al. [45]. In Greer's work the pillars were relatively large with diameters in the micrometer range, whereas Nagel produced pillars of 100 nm in diameter and 285 nm in height. Today, electrochemical deposition of gold nanopillars onto different template materials is well established and widely used for applications such as cell interfaces [46, 47], plasmonic devices [48], and electrodes for glucose detection [43, 49–51].

Electroless Plating

Electroless gold plating is a very simple and versatile fabrication method for vertical gold nanostructures that was introduced by Menon et al. in 1995 [52]. The templates for electroless deposition do not need to be electronically conductive because they do not serve as functioning electrodes: thus, nonconducting nanostructured polymer membranes are used, for example [22, 31]. In this approach a catalyst is required, which acts as a molecular anchor at the pore walls; Martin et al. used Sn^{2+} to sensitize the membrane [30]. In the following redox reaction involving $AgNO_3$, Ag nanoparticles are deposited at the pore walls: when this coated membrane is placed in a gold plating bath, the Ag particles are galvanically displaced as Au is the more noble metal [52]. The metal deposition starts at the pore walls and proceeds uniformly down through the complete pore length. Thus, nanopillars up to 10 μm can be deposited, longer than nanotubes resulting from other template-assisted methods. Depending on the pore length of the polymer template, the production of longer gold nanopillars up to 50 μm is possible [37]. For short deposition times hollow metal tubules are obtained, whereas longer deposition times of up to 48 h lead to the formation of solid gold pillars [31, 53]. Gold nanotubes or pillars with diameters from 10 nm [52, 54] to 460 nm [55, 56] have been prepared by electroless plating. Currently, this method is primarily applied to the fabrication of gold electrodes with hollow nanotubes or solid nanopillars [42, 56–59].

Physical Vapor Deposition

Physical vapor deposition (PVD) into track-etched polycarbonate membranes was considered by Brumlik et al. as another fabrication method for gold nanostructures [37]. However, they did not obtain solid gold nanorods with this technique but rather hollow tubules, which they subsequently strengthened electrochemically. Anandan et al. also used PVD to prepare silicon nanopillars from AAO templates [60]: when Si wires were exposed to water to test applicability in biosensors, severe bending of the nanostructures due to capillary forces occurred (see section 'Mechanical Stability'). They concluded that PVD would not be a suitable fabrication method for gold nanopillars used in biosensing applications as this method results in nanopillars of insufficient mechanical strength. Instead, cost-effective electrochemical template synthesis was recommended, which resulted in more mechanically stable gold nanorods.

Focused Ion Beam Milling

Focused ion beam (FIB) fabrication techniques involve the use of a beam of heavy ions, typically Ga+, to selectively and nonreactively etch a surface [61]. The technique may be used to trace geometric patterns on the tens of a nanometer scale, depending on the quality of the control systems of the particular instrument. The finesse of the resultant structures is typically limited by the quality of the ion optics, the Gaussian distribution of the incident focused ion beam, parameters and systems used to trace the design, and thermal- and charge-induced drift of the sample image position. Charge compensation using a local electron flood gun can act to mitigate image drift and distortion to a certain extent, while sectioning for depth profiling can be performed by the formation and polishing of a trench [61]. Reactive gas may be injected for local etching, as well as deposition of metal such as platinum in order to provide a scaffold for nanostructures that might otherwise be damaged during sectioning.

Dual-beam instruments combine a scanning electron microscopy (SEM) and FIB column to permit in situ forming and imaging by both ion and electron beams; the FIB column is commonly mounted at an oblique angle to the vertical SEM column, permitting concurrent SEM and FIB manipulation at an appropriately eucentric position on the sample. Ion beam imaging may be implemented as an alternative microscopy contrast to that of SEM, but one must be aware that sample etching occurs concurrently, and thus one must optimize parameters to avoid sample degradation [61]. A schematic example of the dual-beam FIB setup is shown in Fig. 11.2 below, where the main features of the apparatus are highlighted.

FIB milling is well suited to the manufacture of gold nanopillars, including individual pillars for mechanical testing, and arrays of pillars for device style applications [24, 62–65]. A multistep FIB milling procedure has been developed that is suitable for the fabrication of gold nanopillars of complex geometries [28]. Seeding of pattern array positions or templates for epitaxially grown structures is also possible by FIB methods, as regular arrays can be laid down on a surface with a high degree of automation. The diameter of FIB-milled gold nanopillars may range from 50 nm [28] to 8 μm [62] and thus spans a much larger range than template-assisted synthesis. With 30 nm [28] to 11 μm [62] the height range is comparable (see Table 11.1).

Negative issues that could arise during the use of FIB fabrication techniques include the implantation of heavy ions, the formation of defects, and an amorphous surface layer [44, 61, 66]. The nature of such an amorphous layer and precipitation of gallium at the sample surface has been investigated by Lehrer et al. [67], where they found the implantation depth depends on the energy of the incident ions and may be up to 70 nm below the surface. With regard to milled nanopillar structures, one should also be aware of lateral contamination due to redistribution of sputtered gallium and sample particulates from the milling process.

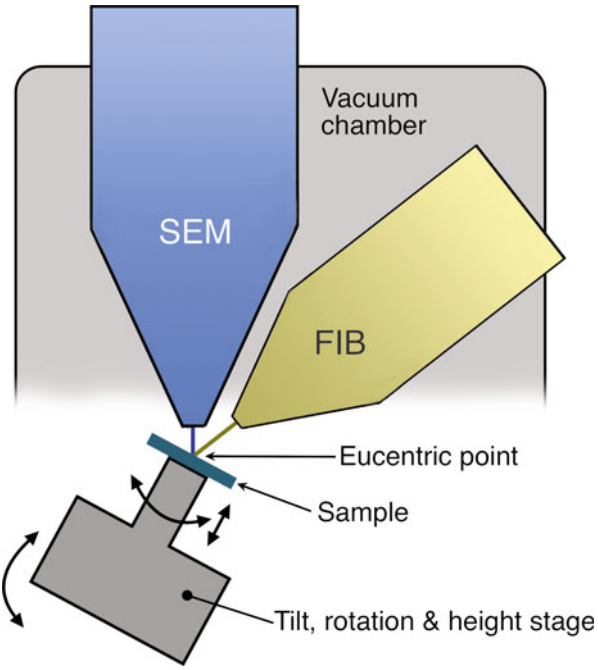

Fig. 11.2 Schematic of a dual-beam FIB/SEM setup, illustrating a vertical SEM column and tilted FIB column, both incident on a eucentric working area on the sample

Nanoimprint Lithography

Nanoimprint lithography (NIL) by both hot and cold embossing is another promising route to the fabrication of uniform nanostructures over large areas. One generally considers the imprint of a high-stiffness, nanopatterned mold into a soft layer under the influence of pressure and/or temperature, either directly over a single area or in a roll-to-roll process [68]. By such methods one can rapidly produce large nanopatterned areas with applications in the field of biology, photoresists, and photonics, for example [69]. The malleability of gold facilitates NIL embossing as a feasible method for the production of gold nanopillars; the lithographic imprinting of gold by a prefabricated patterned master (e.g., by lithographic writing onto silicon) can produce high-fidelity nanopillars for various applications [20, 63, 70, 71]. A wide range of geometries are feasible depending on the quality of replication; to date gold nanopillars were fabricated via NIL in a much narrower geometry range than FIB-milled nanopillars (see Table 11.1). The diameters of imprinted gold pillars range from 100 to 1,100 nm with heights between 50 and 4,000 nm.

For certain applications imprinted gold nanopillars may be modified after the imprinting process. Gao et al. fabricated a large array of 300 nm diameter gold nanopillars with 1:1 aspect ratio via NIL, which they subsequently coated with Fe_2O_3 to enable plasmonic applications [71]. It is also possible to deposit gold onto

polymeric nanopillars produced by NIL in order to form active systems for plasmonic sensing [72, 73]. Nakamoto et al. fabricated nanopillar-hole structures for plasmonic nanogap devices [70], where nanoholes consisting of polyethylene terephthalate were fabricated via NIL followed by sputtering gold into the holes. This process led to the formation of one nanopillar in each hole, due to selective gold deposition at the base of the hole and upper edge of the surrounding polymer. Almost defectless nanopillar-hole pairs were fabricated over an area of several square millimeters. Nanopillar height and the gap between pillar and hole could be controlled by tuning the hole depth and sputtering time.

Other Fabrication Techniques

Gold nanopillars can also be fabricated by electron beam (e-beam)-induced decomposition of an organometallic precursor [28]. Dhawan et al. used an e-beam to dissociate gold from the precursor gas dimethyl Au (III) fluoro acetylacetonate. The necessary ionization energy was in the range of the secondary electrons (between 5 and 50 eV), generated when the glass substrate was exposed to a focused e-beam. The glass substrate was coated with either indium tin oxide (ITO) or Ti, as the negative surface charge of uncoated glass would deflect the e-beam. Linear arrays of gold nanopillars, with diameters between 40 and 70 nm and spacing between 15 and 30 nm, were fabricated by this process. In future developments, such linear gold nanopillar arrays on coated glass could find applications as plasmonic waveguides.

A novel fabrication method for gold nanopillars based on the assembly of Au nanoparticles was recently presented by Cetin et al. [27]: a mask of poly(methyl methacrylate) (PMMA) on a gold substrate was structured by e-beam lithography to form nanopores; these nanopores were subsequently filled with gold nanoparticles suspended in deionized water (see Fig. 11.3). By applying an electric field, the nanoparticles were fused together to form nanopillars, and upon removal of the PMMA mask by dissolution with acetone, freestanding gold nanopillars with diameters between 50 and 100 nm and heights up to 400 nm remained. Changing the mask geometry will also enable the assembly of Au nanoparticles into pillars of other dimensions. Appropriate applications for such Au nanopillars would be in optical trapping or biosensing nanoplasmonic devices, for instance.

Fabrication of Prepatterned Nanopillars

Often, the fabrication of gold nanopillars is combined with a patterning method to create arrays of gold nanopillars with specific geometric constraints and long-range order. A simple approach for the fabrication of localized gold nanopillars is the combination of e-beam lithography and metal deposition. Zin et al. used this approach to produce gold nanopillars on Si wafers that were prestructured by e-beam lithography of a PMMA resist followed by a lift-off process [25]. The resulting gold

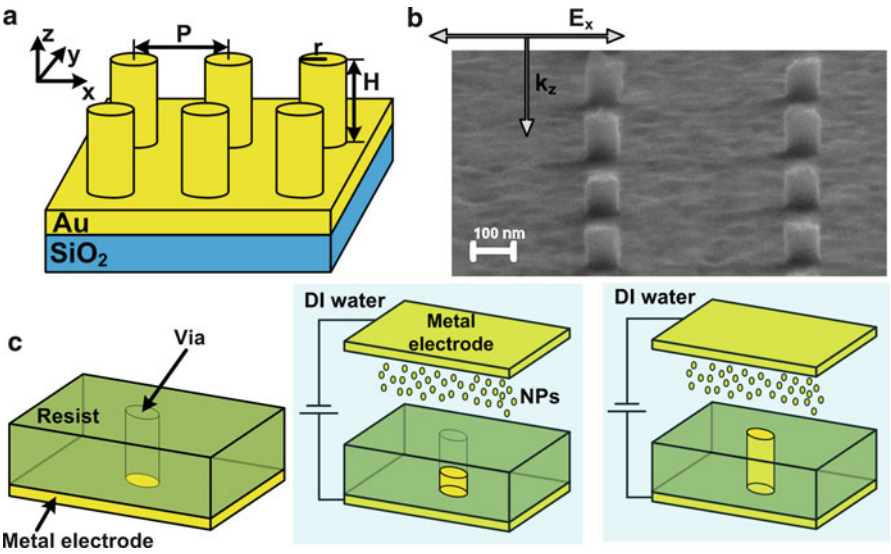

Fig. 11.3 Gold nanopillars prepared by assembly of gold nanoparticles. (**a**) Geometry of the nanopillar arrays. (**b**) SEM image of the nanopillar array with radius 50 nm, height 100 nm, and pitch 500 nm. The direction of propagation and polarization of the illumination source is indicated in the figure. (**c**) Fabrication process of the nanopillar arrays (Reprinted with permission from [27], copyright 2011 AIP Publishing LLC)

nanopillars had diameters ranging from 50 to 200 nm, where the height was maintained at 50 nm. Due to the prepatterning of the Si wafer, periodic arrangements of pillar bundles were achieved with grating constants from 50 to 200 nm. These patterns could be fabricated with a precision of 20 nm on a large scale up to $10 \times 10\ \mu m^2$. Nagel et al. also used this approach to create a cubic lattice of single-gold nanopillars with a height of 285 nm and a diameter of 100 nm [45]; the pitch of this lattice was adjusted to 250 nm.

Combining imprint or lithography methods with template-assisted synthesis also enables the fabrication of localized gold nanopillars at predefined positions on a substrate. This technique has been employed for the production of large-scale nano- and micropatterned gold nanopillar arrays on silicon substrates [74]. First, Si wafers were coated with 500 nm of aluminum, onto which different micropatterns were imprinted using silicon stamps that were prestructured by lithography combined with reactive ion etching (RIE). After transferring the micropattern onto the Al film, anodization was carried out to obtain nanoporous AAO membranes, which were electrochemically filled with Au at the predefined positions. The resulting gold nanopillars were 35 nm in diameter and 300 nm high.

Later, Matéfi-Tempfli et al. realized the growth of localized gold nanopillars by combining template-assisted deposition onto AAO templates with two different photolithography methods [75]. In one approach AAO membranes were prepared on a confluent gold layer, subsequently coated with 100 nm of SiN, and finally

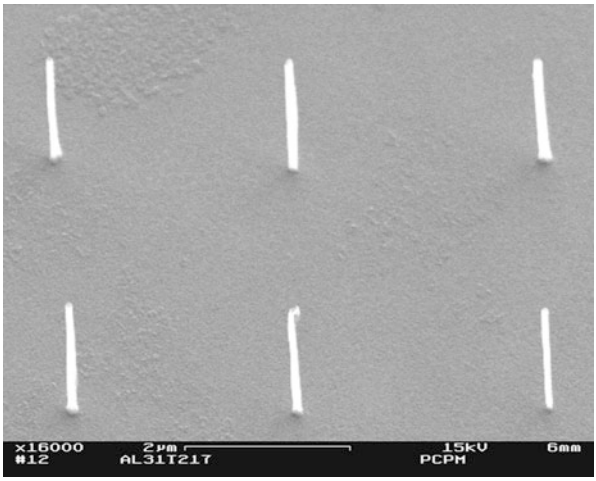

Fig. 11.4 Scanning electron micrograph of localized single nanowires in a matrix arrangement, fabricated by the masking of the supported nanoporous alumina surface using e-beam lithography. Image courtesy of A. Vlad (unpublished)

PMMA was deposited on the SiN and prestructured by e-beam lithography. After resist development and RIE, the SiN layer was patterned and gold was deposited into the selectively opened nanopores. This technique exhibited a very high precision, which allowed for the production of freestanding gold nanopillars at widely spaced, predefined positions, as can be seen in Fig. 11.4.

In an alternate fabrication method, a gold layer upon a Si wafer was prestructured via lithography before Al was deposited and anodized to obtain nanopores. During the subsequent electrochemical gold deposition, the pillars only grew on the localized conducting parts of the underlayer [75].

Recently, Weber et al. adapted this lithography approach of a metal layer under the AAO membrane by depositing a sandwich structure of a gold film, a titanium barrier, and an upper gold film on Si [76]. Circular gold patches with diameters from 100 to 600 nm were patterned on the upper gold layer using e-beam lithography into a PMMA resist followed by a lift-off step. Subsequently, an Al film was deposited and anodized, followed by electrochemical filling of the AAO nanopores yielding gold nanopillars in the predefined circular positions. The rest of the surface was masked by the Ti barrier layer meaning the associated pores were not filled with gold. Prestructuring of the underlying gold substrate could also be achieved by FIB milling, as suggested by Einsle et al. [77]. Certain areas of the gold layer may be removed with the ion beam, and the size of these areas could be adjusted to the diameter of single AAO pores. Subsequent aluminum deposition, anodization, and pore filling yielded gold nanopillar arrays with scalable pillar densities and tailored heights.

A combination of e-beam lithography and template stripping to fabricate localized areas of gold nanopillars was recently introduced by Wang et al. [78]. In this approach, a silicon template was produced by e-beam lithography and RIE, followed by the deposition of 500 nm gold and 1,000 nm copper. The copper layer was topped by single-crystal silicon, which was then used to strip the gold structure from the underlying template [48]. The resulting single gold nanopillars of diameter 280 nm

and a height of 130 nm were extremely regular in shape and of a smoother surface than gold nanopillars fabricated by the standard lift-off process [78]. As an illustration of the application of these gold nanostructures, plasmonic trapping of small polystyrene particles was demonstrated by Wang et al. [48, 78].

Properties

Gold nanopillars have been found to exhibit a wide range of material properties, combining excellent optical properties, based on surface-plasmon resonance (SPR), as well as good electrical conductivity. Due to their chemical inertness, gold nanopillars are also biocompatible and favorable as biointerfaces. In this section we present a detailed overview of the versatile properties of gold nanopillars.

Mechanical Stability

Mechanical properties of nanoscale structures are well known to deviate from those of the bulk, exhibiting size effects across a wide range of properties [62]. Nanopillars fabricated of metal and dielectric materials, in both amorphous and microcrystalline states, generally fall under the banner of 'smaller is stronger' [44]. The result of this size effect is that metallic nanopillars often exhibit mechanical properties of an increased magnitude: typically the moduli (relating elastic properties) and yield strength (the minimum stress required to induce plastic deformation) both increase with respect to the accepted bulk values, the mechanisms for which shall be considered further in this section.

Uniaxial compression testing of individual gold nanopillars has been accomplished to a high level of accuracy using instrumented nanoindenter apparatus [63, 65], as shown in Fig. 11.5, for example: a diamond flat punch of a diameter larger than the pillar is brought into conformal contact with the pillar in a load-controlled regime, while load–displacement data are gathered during loading to compressive failure. This 'smaller is stronger' refrain is ably demonstrated to be valid for gold nanopillars tested under uniaxial compression: the ultimate compressive yield stress has been shown to increase from the bulk value of around 30 MPa to as high as 800 MPa, an effect that has been attributed to dislocation starvation [24, 66]. Other size effects are also manifested: for example, it has been demonstrated for both as-produced and prestrained/annealed gold nanopillars that the yield stress is reduced (typically by up to around 50 %) by prestraining, an effect not seen in the bulk and a result of increased dislocation density and reduced flow stress [64]. No significant differences were found when comparing gold nanopillars produced by FIB milling and NIL fabrication methods with regard to mechanics and scaling behavior [63].

The mechanical stability of gold nanopillars is particularly important for applications where they are exposed to electrolytes or buffer solutions, such as in biocompatibility studies, for example. Anandan et al. used a water droplet test to

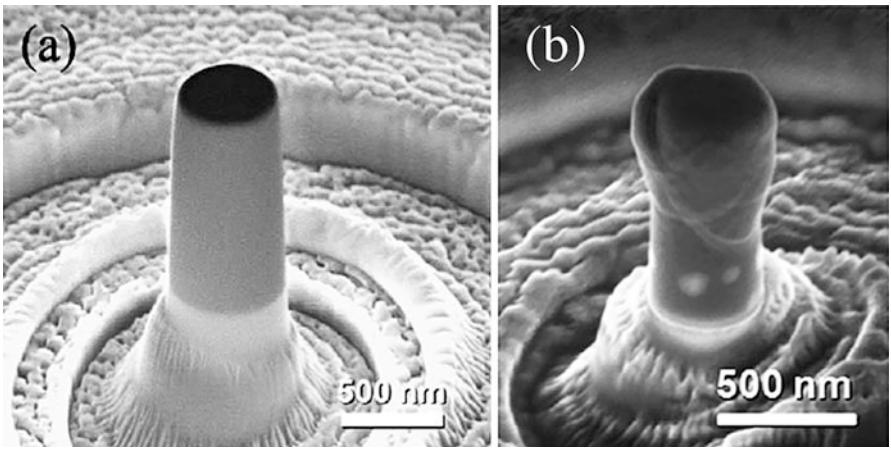

Fig. 11.5 Scanning electron micrographs illustrating the uniaxial compression testing of a FIB milling-fabricated Au nanopillar in an instrumented nanoindenter (**a**) prior to, and (**b**), post compression: the slip boundaries that form at the surface propagate across the pillar causing failure (Reproduced from [64], copyright 2009 Elsevier Ltd.)

study how gold nanorods behave in a liquid environment [60]. The pillars were fabricated via AAO template synthesis and were of 150 nm in diameter and 4.5 μm high, thus yielding an aspect ratio of 30. After the AAO template was removed, the nanopillars showed slight bunching at the free ends. The subsequent water droplet tests did not deform the pillars any further; Anandan et al. concluded that the pillar bending occurred due to capillary forces between the nanostructures and the electrolyte. For gold nanopillars with aspect ratios below 30, no deformation was observed: thus, gold nanopillars of lower aspect ratios exhibit a higher resistance to bending, which is important in cell culture or electrochemical studies where the nanopillars are exposed to liquids (see sections 'Biocompatibility' and 'Electrochemical Properties').

Crystalline Microstructure

Gold nanopillar volumes are sufficiently small such that one may turn to molecular dynamic (MD) simulations to provide some information on the anomalous behavior observed in nanopillar mechanics. MD simulations of defect-free gold nanopillars of only a few nanometers in diameter indicate that dislocations are nucleated on the exterior surface of the nanopillar [79]. Similarly, simulations of dislocation motion through single nanopillars with diameters below 10 nm have shown that when the diameter falls below a certain critical length scale, the onset of slippage (dislocation motion within a crystal plane) is governed only by the free surface rather than the bulk of the pillar [80]. Bulk metallic glass nanopillars – amorphous states of metal with no crystalline structure – exhibit a lesser magnitude of size effect on the yield strength compared to microcrystalline metallic nanopillars [81]. The Young's modulus of

multishell gold nanowires under compression is shown to increase with decreasing radius by MD simulation [82]. Simulations also indicate that the formation of nanotwinned grain boundaries in gold nanopillars – where the atomic structure is mirrored on either side of the boundary – results in an increase of mechanical strength [83].

The crystalline structure, orientation, and grain boundaries within gold nanopillars may be experimentally probed by suitable techniques, including scanning and transmission electron microscopy (SEM and TEM), X-ray diffraction (XRD), and photon correlation spectroscopy (PCS). TEM was utilized by Lancon et al. to show that incommensurate surfaces at <100> slip boundaries in gold nanopillars lead to frictionless sliding at that boundary [65]. Schneckenburger et al. showed with high resolution TEM that electrochemically deposited gold nanowires with <111> orientation had a homogenous, monocrystalline and low defect nature [153]. Crystalline gold nanotubes and nanorods with <111> orientation on titanium foils were also analyzed by Wang et al. using TEM and XRD to study the respective growth mechanisms in PC templates [154]. Shin et al. and Cherevko et al. used energy-dispersive X-ray spectroscopy, field emission SEM, and XRD to characterize the surface morphology and chemical composition of gold nanopillar arrays for electrochemical sensor applications [49, 51]. Similar techniques were used by Forrer et al. to characterize gold nanowire arrays formed by template synthesis [42].

Crystal orientation plays a significant role in the mechanics of gold nanopillars: for example, the onset of plasticity in <111>−oriented gold nanopillars is shown by atomistic simulation to depend on the binding of the surface atoms [84]. Diao and coworkers have studied the yield mechanisms in gold nanowires by atomistic simulation and show that nanowires yield via the propagation of <112> dislocations [85, 86]. Further MD simulations by Weinberger and Cai comparing body-centered cubic (BCC) and face-centered cubic (FCC) gold pillars indicate that single dislocations may multiply within a BCC micropillar but not an FCC pillar [87].

Plasmonic and Optical Characteristics

Surface-plasmon resonance is a property commonly observed in metals, whereby the electrons at the surface oscillate collectively in response to incident light. Gold is strongly plasmonically active, and the frequencies at which the plasmon resonance interacts with the incident light may be tuned via control of nanoscopic length scales. One may witness this effect in gold nanoparticle suspensions, whereby with decreasing particle diameter the observed color of the nanoparticle suspension becomes distinctly blue and then red, depending on the wavelengths of light absorbed by the plasmonic interaction [1].

The same degree of control over surface-plasmon interaction may be replicated by patterning gold with nanopillars of various diameters. Plasmonically active gold nanopillar arrays – with the requisite varying diameters – may be formed by the nanoimprinting of gold nanoparticles from a PDMS stamp, as demonstrated by Liang et al. [69]. Wurtz et al. proposed the use of plasmonic properties of gold

nanorod arrays for ultrafast optical device applications [88]. Furthermore, gold nanopillar surfaces are suitable for forming surface-plasmon traps and waveguides, as presented in recent studies [28, 48, 71]. Metamaterials, such as AAO membranes with embedded gold nanopillars (see section 'Metamaterials'), can also be applied to non-plasmonic optical applications: Pollard and coworkers have, for instance, demonstrated a number of applications utilizing the optical extinction spectra of such metamaterials by experiment and theoretical modeling [40, 89].

Biocompatibility

During the past few years, cell-nanostructure interfaces have become increasingly important in various nanobiotechnology applications, including cell signaling for improved cell adhesion and the development of novel implant materials [90, 91]. All these applications require the respective nanomaterial to be biocompatible so cells may adhere to the nanotopography showing vital growth.

Gold nanopillars have been found to exhibit biocompatibility towards several cell types. The first cell culture experiments on gold nanopillars were presented in 2007 by Haq et al. using the neuron precursor cell line of rat pheochromocytoma (PC-12) [92]. The nanopillars were fabricated using electrodeposition onto AAO templates of 200 nm in diameter, 2 μm high and spaced 70 nm apart, dimensions comparable to the size of cellular filopodia. A poly-L-lysine coating on top of a self-assembled monolayer (see section 'Self-Assembled Monolayer Coatings') was used to promote cell adhesion, and the PC-12 cells were found to adhere and proliferate on the coated nanopillars. However, the cells developed fewer and shorter neurites on the nanopillar substrates than on smooth reference surfaces, indicating the PC-12 cells were spatially aware of the underlying nanotopography. In future, gold nanopillar substrates may act as a useful tool in controlling neurite development in neurons.

In a later study gold nanopillar electrode arrays of 8–20 μm in diameter were coated with the protein fibronectin (see section 'Protein Modifications') and used for extracellular recordings from the cardiac muscle cell line HL-1 [46]. The gold nanopillars were of 300–400 nm in height and 60 nm in diameter. In this geometry the pillars supported tight adhesion of HL-1 cells, while the cell membranes also followed the underlying nanotopography. The distance between cell membrane and pillar tips was found to be $\leq$ 100 nm, as shown in Fig. 11.6. However, the membrane did not bend around the pillars or incorporate the nanostructures in any way. When the same pillar geometry was used for large-scale gold nanopillar arrays in detailed cell adhesion studies, HL-1 cells protruded into the inter-pillar cavities with diameters below 100 nm for the first time [47]. Furthermore, gold nanopillars were found to support vital growth and tight adhesion of the human embryonic cell line HEK 293. Gaps between pillar tips and HEK cell membranes were low, with distances generally below 200 nm. It was also observed that not only did cells react to the underlying nanotopography but bending of the nanopillars also occurred with HL-1 and HEK cells adhered to the arrays; nanostructure bending was presumably driven by cell adhesion forces.

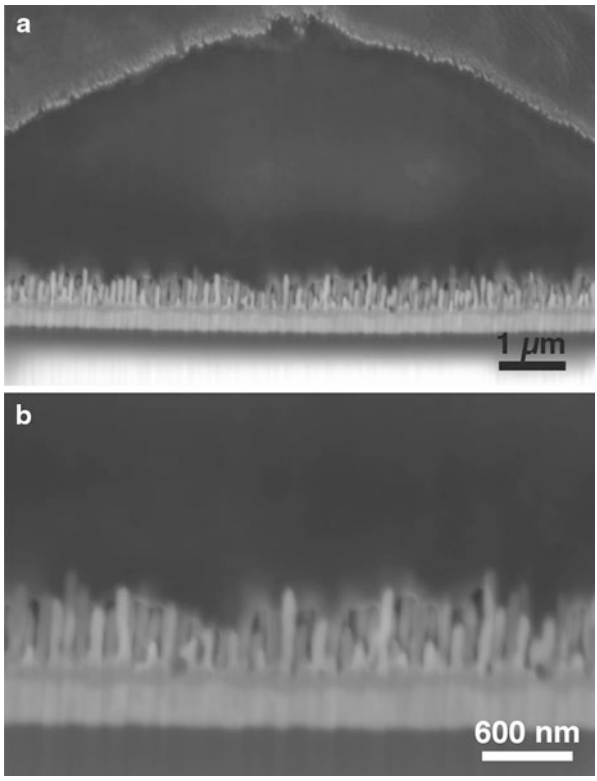

Fig. 11.6 Tight adhesion of HL-1 cells to gold nanopillars. (**a**) Overview on the cell-nanopillar interface. (**b**) Detailed view of the HL-1 cell membrane protruding into the inter-pillar regions (Reproduced from [47], copyright 2012 Inderscience)

When primary cortical rat embryonic neurons (RCN) were grown on gold nanopillar arrays that had been coated with distinct self-assembled monolayers (see section 'Self-Assembled Monolayer Coatings'), a different scenario was observed [47]. Adhesion and viability of RCN were unexpectedly low with large distances between neuronal cell bodies and nanopillars. Actin assembly in the neuronal growth cones was modified on gold nanopillars, thus indicating changes in the neuronal cytoskeleton leading to a reduction in adhesion. These observations were independent of the respective self-assembled monolayer coating; thus, it was assumed that the nanopillar geometry is the key parameter for neuronal adhesion and proliferation. Changes in the geometry might enable vital neuronal cell growth on gold nanopillars in future studies.

Electrochemical Properties

Over the last decades, the development of new micro- and nanoscale electrode designs has been largely motivated by electrochemical investigations. For example, studies on neuronal chemical communication, such as the observation of vesicular neurotransmitter release from individual cells, require the use of tiny electrodes to

achieve the desired spatial resolution on a (sub)cellular level [93–95]. Apart from the benefit of performing localized electrochemical experiments, such as the investigation of single cells, nanoscale electrodes allow the exploration of fundamental electrochemical phenomena, due to the fast diffusive processes that occur on the nanometer scale. The possibility to fabricate and employ such electrodes has facilitated the study of rapid electron-transfer reactions that are not accessible using conventional macroelectrodes [96, 97]. Furthermore, the small dimensions and associated small interface capacitances of such electrodes make it possible to carry out electrochemical measurements in highly resistive media and to observe phenomena on a submicrosecond time scale [98–100]. First band electrodes that were confined at least in one dimension to the nanoscale were developed and tested during the 1980s by several groups [101–103]. Since then, a huge variety of different approaches for both fabricating and applying nanoscale electrodes has been implemented [104–108]. In this context, not only the size of the electrodes but also the distance between individual electrodes has been scaled to the nanometer range. This is particularly interesting for redox-cycling applications, where closely spaced electrodes are independently biased to subsequently reduce and oxidize a molecule of interest [109]. The electrochemical amplification associated with redox cycling on the nanoscale has been exploited in a variety of applications, including scanning electrochemical microscopy (SECM) [110–116] and the electrochemical detection of single molecules [117–122]. On-chip redox cycling techniques for electrochemical sensing applications can profit from versatile nanofabrication technologies [123]. In the future, individually addressable nanopillar electrodes might further advance the implementation of highly efficient redox cycling concepts for electrochemical applications.

Metal nanopillars fabricated by template deposition as described above (see section ‘Template-Assisted Synthesis’) fall into a special category of nanoelectrode ensembles [52]. Typically, all nanoelectrodes are addressed at the same time, and template materials that exhibit densely packed nanostructures, such as AAO membranes, result in pillar arrangements whose distances lie in the submicrometer regime. Consequently, in most electrochemical experiments the diffusive field of individual pillar electrodes will overlap, as shown in Fig. 11.6, where various different diffusion mechanisms are depicted. The resulting ‘macroscopic’ diffusion layer and steady-state Faradaic currents are dominated by the geometric aspects of the electrode itself and not by the individual structure of the nanopillars. Macroscopic nanopillar modified electrodes thus exhibit ‘classical’ peak-shaped voltammograms, instead of the diffusion-limited sigmoidal shapes observed with individual ultramicro- or nanoelectrodes that exhibit radial diffusion profiles (see Fig. 11.7). However, there is a striking difference between conventional planar and nanopillar modified macroelectrodes. As the mass transport at the tip of an individual nanopillar is enhanced, kinetic effects of the electrode reactions play a greater role compared to reactions occurring at a planar surface. This makes it possible to study fast electrode kinetics not accessible in experiments employing planar macroelectrodes. Furthermore, if the shafts of the nanopillars are insulated, then the overall exposure of the electrode material to the electrolyte is strongly reduced without altering the geometric

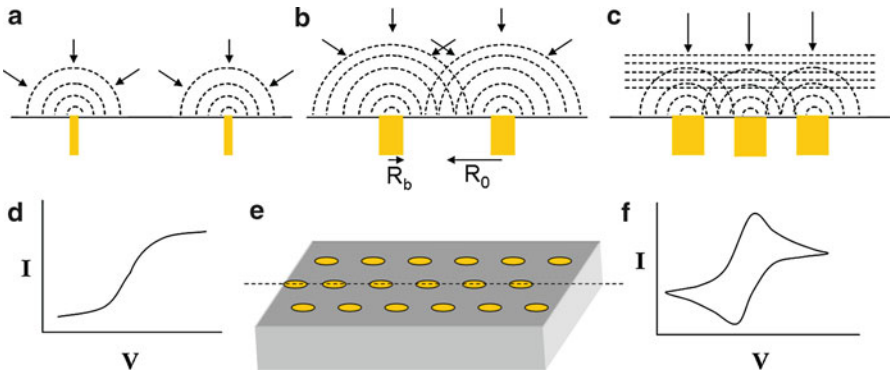

Fig. 11.7 Schematic of electrode ensembles of different size and density showing (**a**) radial diffusion, (**b**) overlapping radial diffusion, and (**c**) planar diffusion. (**d** and **f**) Cyclic voltammograms for the diffusion scenario in (**a**) and (**c**), respectively. (**e**) Electrode ensemble with metal electrodes represented by yellow circles surrounded by gray insulating material. Microelectrode radius, R_b, and diffusion zone radius, R_0, are shown (Reprinted with permission from [134], copyright 2008 American Chemical Society)

dimensions of the electrode. As a result, we obtain a decrease of the double-layer capacitance and corresponding increase in the electrode impedance, which reduces the background noise in current measurements. Additionally, the low capacitance yields fast response times without compromising the sensitivity of the electrode via an effective geometric area reduction. Martin and coworkers have exploited this effect in their pioneering work on gold nanoelectrode ensembles [52, 124]. They demonstrated a reduction of the detection limit for redox-active molecules exhibiting fast electron-transfer kinetics by three orders of magnitude at a gold nanoelectrode ensemble. A variety of approaches based on this principle and related techniques have evolved since then, not only with gold nanopillars but also with carbon nanotubes, magnetic nanowires, or polymeric and semiconductor nanostructures [54, 58, 59, 125–135]. While most of these methods aim at increasing the ratio of Faradaic to capacitive currents, some applications do require the opposite, namely, the presence of a large interfacial capacitance at small geometric dimensions. This is particularly interesting for highly localized voltage measurements of electrophysiological signals such as extracellular recordings of action potentials from single cells. Gold nanopillar electrodes can also meet this requirement if the shafts and not only the tips are exposed to the electrolyte solution [42, 46, 50, 136–138]. Such a configuration effectively lowers the electrode impedance without altering its geometric size and can additionally enhance the coupling between cell and electrode. In fact, this and similar concepts are currently pursued for the development of novel neurotechnology interfaces [5, 7, 8, 46, 47, 138–142]. Other applications of gold nanopillars make use of exposed pillars to increase the apparent electrode kinetics, or the loading capacity for specific enzymes, to improve the electrochemical sensing performance [41, 50]. Electrochemical characteristics of different studies on gold nanopillars are summarized in Table 11.2.

Table 11.2 Electrochemical properties of gold nanopillar electrode systems with different geometries

Nanopillar geometry	Electrochemical characteristics	References
Gold nanowire arrays, electropolished in 1 M H_2SO_4 (100–800 nm long, tip diameters of 30–80 nm)	Measured by cyclic voltammetry in Na_2SO_4, gold nanowires show a surface increase factor of 90 compared to flat gold electrodes	Forrer et al. [42]
Gold nanopillar microelectrodes (8–20 μm diameter) with pillars of 300–400 nm length and 60 nm diameter	Impedance of gold nanopillars in NaCl is reduced by one order of magnitude compared to planar gold electrodes	Brüggemann et al. [46]
Gold nanorod electrodes on flexible polyimide film: pillar diameter of 50–200 nm and height between 300 nm and 1 μm	Impedance of gold nanorods in NaCl is 25 times lower than the impedance of planar gold electrodes	Zhou et al. [138]
Gold nanopillars of 150 nm diameter with 4.5 μm height	Charging currents in Na_2SO_4 are 38 times higher than for flat gold electrodes. With the redox-active molecule $K_4Fe(CN)_6$, a sevenfold increase in sensitivity compared to flat gold electrodes is obtained	Anandan et al. [60]
Gold nanopillars with 150 nm diameter and heights between 1 and 6 μm	Sensitivity of nanopillar electrodes to the redox molecule $K_4Fe(CN)_6$ in Na_2SO_4 is increased by a factor of two compared to flat gold	Anandan et al. [50]
Gold nanopillars with 50 nm diameter and 200 nm height	Surface increase factors between 1.5 and 11.3 for different capacity and charge transfer-based systems	Schröper et al. [136]
Gold nanopillars of 200 nm diameter and 4 to 22.5 μm length on microelectrodes (10 to 40 μm diameter)	At 1 kHz impedance is reduced by a factor of 89.5	Nick et al. [156]

Functionalization and Surface Modification

A variety of surface functionalization methods have been introduced for gold nanopillars to facilitate their use in applications such as biosensors and cell interfaces. Established surface modifications ranging from self-assembled monolayers, proteins, and polymers to metal oxides are presented in this section. Furthermore, we discuss gold nanopillars that have been incorporated into other materials to form metamaterials with novel properties.

Self-Assembled Monolayer Coatings

Self-assembled monolayers (SAMs) can reproducibly immobilize, orientate, and organize biomolecules on various metal surfaces through different functional head groups. SAMs are widely employed as anchoring molecules for modifications of gold nanopillars in cell culture and biosensing applications.

Table 11.3 Overview on self-assembled monolayers, which have previously been used to modify gold nanopillars for various applications

Self-assembled monolayer	Applications	References
2-Mercaptoethylamine 3-Mercaptopropionic acid	Enzyme electrode fabrication for amperometric detection of glucose and H_2O_2	Delvaux et al. [55, 56, 143]
3-Mercaptopropionic acid 11-Mercaptoundecanoic acid	Glucose sensing: reaction kinetics and influence of SAM chain length Biotin/avidin detection system	Anandan et al. [41, 50, 144]
2-Mercaptoethylamine, coated with poly-L-lysine	Growth promoting coating for PC-12 cells	Haq et al. [92]
$HS(CH_2)_{11}NH_2$ and mixed monolayer consisting of $HS(CH_2)_{11}EG_3$ and $HS(CH_2)_{11}EG_6NH_2$	Growth and adhesion promoting coating for neuronal cell cultures	Brüggemann et al. [47]
2-Mercaptoethylamine as substrate for gold nanopillars	Electrochemical sensors	Wang et al. [145] and Shin et al. [51]
11-Mercaptoundecanoic acid	Immobilization of the redox protein cytochrome c for electrochemical studies	Schröper et al. [136]
Thiophenol	Surface-enhanced Raman scattering sensors	Caldwell et al. [152]
10-Carboxyl-1-decanethiol	Highly sensitive plasmonic biosensors	Saito et al. [72]

For gold in particular, alkanethiol SAMs are used, which form a strong covalent bond via chemisorption of an –SH group [21]. Because of this strong bond, it is not possible to remove SAM coatings from gold surfaces and as such they cannot be reused. When used in biosensors, SAMs prevent the close approach of solvents to the electrode surface, which results in a reduction of non-faradaic background currents [56]. The various different SAM molecules applied to gold nanopillars by several research groups are summarized in Table 11.3.

Delvaux et al. first reported the SAM modification of gold nanotube electrodes that had been deposited by electroless plating into track-etched PC membranes. They used a thiolated SAM of 2-mercaptoethylamine (MPE, cysteamine) and 3-mercaptopropionic acid (MPA) to introduce amine and carboxylic functionalities onto Au nanotubes by chemisorption [55, 143]. Aminated MPE layers were activated by the linking agent glutaraldehyde that couples to the enzyme glucose oxidase (GOx), which is responsible for breaking down sugar into its metabolites within cells. The terminal carboxylic acid groups of MPA gold pillars were modified with the activating agents 1-ethyl-3-(3-dimethylaminopropyl) hydrochloride (EDC) and *N*-hydroxysuccinimide (NHS), which enabled further coupling of the MPA-modified nanotubes to GOx. By this procedure it was possible, for the first

time, to covalently immobilize GOx to gold nanoelectrodes [143]. In a later study MPA and MPE monolayers on gold nanotubes were also used to bind the enzyme horseradish peroxidase (HRP) to gold nanostructures for the amperometric detection of hydrogen peroxidase (H_2O_2) [56].

Anandan et al. used MPA-modified gold nanopillars from template synthesis with GOx to study reaction kinetics and mass transport during glucose sensing [50]. By introducing the longer SAM 11-mercaptoundecanoic acid (MUA), they were able to examine in detail how the chain length of the absorbed SAMs affects the sensitivity of glucose detection [41]. GOx was covalently bound to MPA- and MUA-modified gold nanopillars with EDC and NHS. The long MUA chains were found to assemble in a more orderly fashion, with a higher degree of surface coverage and less defects than the shorter MPA chains. However, MPA exhibited a higher sensitivity in glucose detection due to a reduced electron-transfer resistance compared to the long MUA chains. MUA SAMs could also be modified with avidin, which enabled the use of MUA-coupled gold nanopillars as a highly sensitive biotin/avidin test system [144]. An alternative to using SAM-modified gold pillars for GOx functionalization is the conducting polymer polypyrrole (PPy). In a recent study films of GOx/PPy were also electropolymerized onto gold nanopillars to enable glucose detection (see section 'Polymer Functionalization') [43].

Cell cultures are another application area for SAM-modified gold nanopillars. Cysteamine monolayers on gold pillars were coated with the protein poly-L-lysine (PLL) by Haq et al. to promote adhesion and growth of the neuronal cell line pheochromocytoma (PC-12) [92]. In a further study two different kinds of SAMs were used to functionalize gold nanopillars for the growth of primary cortical rat neurons: $HS(CH_2)_{11}NH_2$ and a mixed monolayer consisting of $HS(CH_2)_{11}EG_3$ and $HS(CH_2)_{11}EG_6NH_2$ [47]. Both SAMs yielded a vital neuronal cell growth in short-time cell cultures up to 4 days. However, in cultures lasting up to 10 days, the SAM-coated gold nanopillars were not found to support adhesion and proliferation of the neuronal cells, while planar gold substrates with identical SAMs yielded good cell adhesion and proliferation (see section 'Biocompatibility').

SAM modification of gold nanopillars has also been used for other concepts: in a novel approach a monolayer of cysteamine on a planar gold substrate functioned as an anchor layer for the AAO template synthesis of gold nanopillars of uniform height and diameter [51, 145]. A possible application for gold nanopillars grown on SAMs are electrochemical sensors. In electrochemical studies carboxy-terminated monolayers such as MUA were also employed to immobilize redox proteins such as cytochrome c on gold nanopillar surfaces [136]. Moreover, SAMs were reported to improve the surface-enhanced Raman scattering (SERS) of different nanopillar materials that had been modified with gold capping layers. Thiophenol was, for instance, used as a modification for gold-capped Si nanowires in SERS applications [152]. Recently, gold-capped polymer nanopillars of cycloolefin (COP) were functionalized with 10-carboxyl-1-decanethiol to develop a plasmonic detection system for human immunoglobulin [72] (see section 'Gold Nanopillars in Plasmonic Devices').

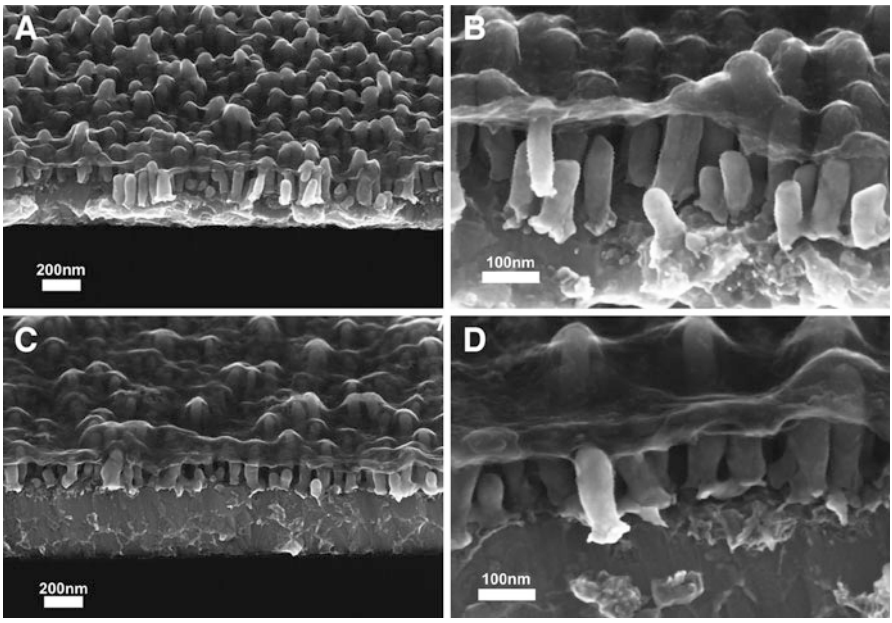

Fig. 11.8 Cross-sectional SEM images of Au nanopillar samples spin coated with PEDOT/PSS. (**A**) and (**B**) show a 28 nm film and (**C**) and (**D**) a 120 nm film in overview and close up. The thinner film adapts better to corrugations of nanopillars than the thicker one resulting in a higher surface roughness for the thinner film (Reprinted with permission from [137], copyright 2011 John Wiley & Sons Inc.)

Polymer Functionalization

Polymer modifications of gold nanopillars have been introduced for many different applications; the conducting polymer PPy was used as an alternative to SAM-modified gold nanopillars for the functionalization with GOx, for example [43]. In this study films of GOx/PPY were electropolymerized onto gold nanopillars for glucose sensing. Another conductive polymer for gold nanopillar modifications is poly(3,4-ethylenedioxythiophene) stabilized with polystyrene sulfonic acid (PEDOT/PSS) [137]. Sanetra et al. spin coated thin PEDOT/PSS films onto gold nanopillars with thicknesses ranging from 30 to 120 nm, completely covering the nanopillars as can be seen in the cross-sectional SEM images in Fig. 11.8. The impedance of these polymer-coated gold nanopillars was reduced by a factor of 2.5 compared to planar gold. In future applications biocompatible conductive polymers could facilitate the use of gold nanopillars as biosensors with improved chemical properties and reduced impedance.

A novel concept of gold-capped polymer nanopillars was recently presented by Saito et al. [72]: an AAO template was used to produce cycloolefin polymer (COP) nanopillars via thermal nanoimprint lithography (NIL) followed by sputter coating of a gold layer of 24–96 nm thick. When the tips of the gold nanopillars were coated with

a 10-carboxyl-1-decanethiol SAM, these structures could be used as biosensors for human immunoglobulin. Since NIL offers the advantage of mass production of polymer nanopillars with reproducible geometries, Saito et al. suggested that gold-capped COP nanopillars will be suitable for industrial and commercial applications in plasmonic biosensing (see section 'Gold Nanopillars in Plasmonic Devices').

Protein Modifications

Protein coatings have been tested for cell culture applications of gold nanopillars alongside SAM modifications (see section 'Biocompatibility'). Recently, gold nanopillar electrodes were coated with fibronectin to enable vital growth and extracellular recordings of the cardiac muscle cell line HL-1 [46, 47]. For cell cultures of human embryonic kidney cells (HEK 293) on gold nanopillars, a modification with PLL was employed, also yielding vital cell growth. Furthermore, PLL has been used as surface modification for cysteamine-coated gold nanopillars to support vital growth and neurite development of PC-12 cells [92]. One advantage of protein coatings versus SAM modifications is that these coatings may be selectively removed with enzymes such as trypsin. This procedure enables the reuse of the underlying gold nanopillar substrates for further cell culture experiments.

In an alternative application of gold nanopillar arrays, a protein-based functionalization strategy was developed to immobilize CdSe-ZnS quantum dots on the pillar tips. Using e-beam lithography and PMMA masks, gold nanoarrays were produced with very precise diameters and interspacing [25]. Three molecules of gold-binding peptide (GBP) formed a consecutive biomolecular linker that was modified with biotin at one end. Streptavidin-modified CdSe-ZnS quantum dots were then coupled to the biotin end of the linker producing structures suitable for surface-plasmon-enhanced fluorescence applications.

Metal Oxide Coatings

A coating of iron oxide was recently deposited onto gold nanopillars through e-beam evaporation [71]. Pillars were coated with 90 nm of Fe_2O_3 using metallic Fe followed by annealing in oxygen. The Fe_2O_3-coated nanopillars were employed as thin-film electrodes for photocatalytic water splitting. Apart from the use of Fe_2O_3 coatings, future experiments could be performed with photoactive materials with wider band gaps such as WO_3 and TiO_2, in combination with nanopillars from other plasmonic metals such as Ag, Al, or Pd.

Metamaterials

Gold nanopillars have also been incorporated into other materials to form composites with tailored properties. A very simple approach to forming such a

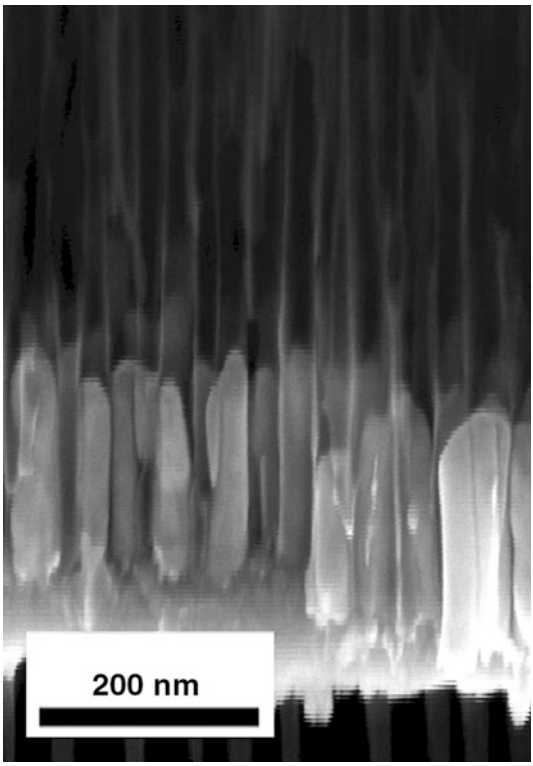

Fig. 11.9 Electrochemically deposited gold nanopillars of 200 nm height in a nanoporous AAO template

metamaterial is the use of template-synthesized gold nanopillars where the AAO membrane is not removed (see Fig. 11.9) [23, 146, 147, 155]. These composites were shown to be transparent in the visible range of the electromagnetic spectrum, and the color of the composite could be tailored by adjusting the diameter of the nanopillars in the AAO membrane [23]. Such AAO/Au metamaterials were also used for plasmonic biosensing with the streptavidin-biotin affinity model [155] and as microhole array electrodes [147]. In later studies AAO/Au composites on glass or silicon substrates and associated optical properties were investigated in more detail, and their application as plasmonic metamaterials with subpicosecond response times was suggested [40, 88, 89].

Composites of polymers and gold nanostructures have also been studied, such as polyester (PES) membranes with embedded gold nanotubes filled with a conductive polymer [148]. The metamaterial was biotinylated to enable coupling with streptavidin-coated microspheres. This model system demonstrated that microtubes could be used as building blocks for the self-assembly of supramolecular architectures. A composite of PC templates and gold nanopillars has also been presented, where a PC-gold composite was etched by O_2 plasma to selectively remove the polymer surface, thus exposing the ends of the gold nanopillars [149]. Since the etch rate of gold is much lower than for the surrounding PC template, the length of

the exposed nanopillars is adjustable by tuning of the plasma etch time. An application of this metamaterial may be nanostructured gold electrodes with tunable surface areas, for instance.

Applications

Gold nanopillars offer outstanding electrochemical and optical properties, good biocompatibility, and a large variety of surface modifications. Because of these excellent properties, they have, for instance, been employed as electrodes in biosensors and into plasmonic devices. We present an overview of recent applications of gold nanopillars within these fields and compare and contrast their respective performance.

Biosensing Employing Nanopillar Electrodes

Electrodes of gold nanopillars were first presented by Menon et al., who used electroless deposition to produce gold nanoelectrode ensembles with individual electrode diameters as small as 10 nm [52] (see section 'Electrochemical Properties'). Several applications of gold nanopillar electrodes in biomolecular sensors and for cell signaling followed this pioneering study. Different gold nanopillar electrode systems with their applications and performance characteristics are summarized in Table 11.4.

Brunetti et al. presented biosensors with hollow gold nanotubes formed by electroless plating. They used gold nanostructures with diameters of 38 nm to develop biosensors based on the enzymes phenothiazine and methylviologen [59]. The resulting nanotube devices exhibited detection limits up to an order of magnitude lower than the detection limit of gold macroelectrodes. With Azure A and Azure B as electron-transfer mediators, the detection limit was as low as 0.12 μM, and for methylviologen 0.2 μM was measured. A later voltammetry study used these nanotube electrodes for trace amounts of (ferrocenylmethyl) trimethylammonium hexafluorophosphate ($TMAFc^+$ PF_6^-) and the protein cytochrome c [58]. The sensors in this work consisted of 4.8×10^6 nanoelectrodes over a total surface of 0.005 square centimeters: detection limits were 0.02 μM for FA^+ and 0.03 μM for cytochrome c. These results opened the path to (bio) sensing applications with gold nanopillars in the submicromolar concentration for the first time.

Today gold nanopillar electrodes are frequently used for the detection of glucose, which has become a model system to study the performance of nanoelectrodes. In amperometric measurements Delvaux et al. first studied the response of β-glucose to gold nanotube biosensors. Hollow gold nanotubes were modified with MPE and MPA to anchor the enzyme GOx above them; in glucose sensing these enzyme-modified gold nanoelectrodes showed a sensitivity of 400 nA mM^{-1} cm^{-2} [143]. In a later study, glucose sensitivities between 50 and

Table 11.4 Performance of gold nanopillars in various biosensing applications

Sensing device	Application	Sensing performance	References
Gold nanodisk electrodes with 10 nm diameter	Voltammetric detection of the redox-active molecule $TMAFc^+$	Detection limit was reduced by three orders of magnitude compared to gold macroelectrodes	Menon et al. [52]; Wirtz et al. [54]
Nanoelectrode ensemble of hollow gold nanotubes	Enzyme detection	Detection limits: 0.12 μM for Azure A and Azure B, 0.2 μM for methylviologen	Brunetti et al. [59]
Nanoelectrode ensemble of hollow gold nanotubes	Voltammetric detection of trace analytes	Detection limits: 0.02 μM for $TMAFc^+$, 0.03 μM for cytochrome c	Moretto et al. [58]
Hollow gold nanotubes with MPE or MPA as anchor for GOx	Amperometric detection of glucose	Sensitivity: 400 nA mM^{-1} cm^{-2}	Delvaux et al. [143]
		Sensitivity: 50–130 nA mM^{-1} cm^{-2} Detection limit: 2×10^{-4} M	Delvaux et al. [55]
Hollow gold nanotubes: bare and with MPE or MPA as anchor for HRP	Amperometric H_2O_2 detection	Bare nanotubes: Sensitivity of 14 μA μM^{-1}	Delvaux et al. [56]
		HRP-modified nanotubes: Sensitivity: 9.5 μA μM^{-1} for MPE and 11.3 μA μM^{-1} for MPA Detection limit: 4×10^{-6} M	
Solid gold nanopillars with GOx on MPA	Amperometric glucose sensing	Sensitivity: 3.13 μA mM^{-1} cm^{-2}	Anandan et al. [50]
Solid gold nanopillars with MPA and MUA for GOx immobilization	Amperometric glucose detection	MPA modification: Sensitivity of 2.68 μA μM^{-1} cm^{-2}	Anandan et al. [41]
		MUA functionalization: Sensitivity of 0.09 μA μM^{-1} cm^{-2}	
Solid gold nanopillars with GOx/PPY	Amperometric glucose sensing	Sensitivity: 36 μA μM^{-1} cm^{-2}	Gangadharan et al. [43]
Solid gold nanopillars without any modification	Nonenzymatic glucose detection: voltammetric and amperometric sensing	Voltammetric detection Sensitivity: 41.9 μA mM^{-1} cm^{-2} Detection limit: below 3×10^{-5} M	Cherevko et al. [49]
		Amperometric sensing Sensitivity: 309.0 μA mM^{-1} cm^{-2} Detection limit: 5×10^{-5} M	
Solid gold nanopillars with avidin on MUA	Avidin-based biotin sensor	Detection limit: 1 ng/ml Sensitivity: 159.0–845.1 $\Omega(ng)^{-1}$ ml mm^{-2} (EIS), 0.521–4.196 $(mFng)^{-1}$ ml mm^{-2} (CV)	Lee et al. [144]
Microelectrodes with solid gold nanopillars	Extracellular signaling with heart muscle cells	Peak-to-peak	Brüggemann et al. [46]
	Signal recording from neurons	Signal amplitudes up to 10 times higher than with planar electrodes	Nick et al. [156]

130 nA mM^{-1} cm^{-2} were reported, where the detection limit was down to just 0.2 mM, and a high reproducibility with standard deviations below 4 % was achieved [55]; at 25 s the response time to the glucose injection was also reasonably fast. Even in the presence of interfering molecules such as ascorbic or uric acid, a linear relationship between glucose concentration and measured current was found for a glucose concentration range between 0.2 and 30 mM.

These same hollow gold nanoelectrodes were used for the amperometric detection of H_2O_2 with and without SAM functionalization. In the presence of a hydroquinone mediator (H_2Q), bare gold nanotubes yielded a sensitivity of 14 μA mM^{-1}, while flat gold macroelectrodes only offered 0.41 μA mM^{-1} [56]. When the gold nanotubes were modified with MPE and MPA, respectively, the enzyme HRP was immobilized on top of them. These HRP nanoelectrodes yielded a slightly lower sensitivity than bare nanotubes, approximately 10 μA mM^{-1} for both SAMs. The lower sensitivity was explained as a decrease of the active surface area during SAM modification and enzyme immobilization. Nevertheless, detection limits down to 4×10^{-6} M were measured for HRP-SAM nanotubes compared to 8×10^{-4} M for flat gold electrodes. When the interfering molecules uric and ascorbic acid or acetaminophen were introduced, the HRP-SAM nanoelectrodes showed the highest selectivity for H_2O_2. Besides their outstanding biosensing performance, these enzyme-modified gold nanotubes have the advantages of low cost, ease of fabrication, fast response time, and good reproducibility.

Anandan et al. later studied the role of reaction kinetics and mass transport in glucose sensing for nanoelectrodes with solid gold nanopillars of different heights (1, 2.5 and 6 μm) [50]. The pillars were of 150 nm in diameter and were functionalized with MPA and loaded with GOx. When 2.5 and 6 μm high nanopillars were wetted during the functionalization process, the nanostructures displayed a slight bunching deformation due to capillary interaction compounded by the reduced flexure rigidity of the higher pillars. The sensitivity of the functionalized pillars to glucose in amperometric current measurements was 0.91, 1.8, and 3.13 μA mM^{-1} cm^{-2} for the 1, 2.5, and 6 μm tall pillars, respectively. The highest sensitivity value for 6 μm high pillars was 12 times greater than the reference result for a flat gold electrode (0.27 μA mM^{-1} cm^{-2}) and almost 8 times greater than the value Delvaux previously reported for hollow gold nanotubes [143]. It was also observed that the larger pillars exhibited longer response times to glucose injection. In another study Anandan et al. investigated the influence of SAM chain length on the sensitivity of glucose detection by functionalizing gold nanopillars with MPA and MUA. The shorter MPA SAM resulted in a higher sensitivity in glucose detection (2.68 μA mM^{-1} cm^{-2}) than the longer-chain MUA (0.09 μA mM^{-1} cm^{-2}) [41]. Since the GOx-catalyzed glucose oxidation is controlled by the position of the redox center relative to the electrode surface, sensitivity also depends on the chain length of the SAM layer: for this reason gold nanopillars with the longer MUA SAM chain exhibited reduced sensing performance compared to MPA. This trend was confirmed for planar gold modified with MPA and MUA, yielding 0.47 and 0.05 μA mM^{-1} cm^{-2}, respectively.

Gold nanopillars of 150 nm in diameter and heights ranging from 1 to 8 μm were also modified with films of GOx/PPY for improved glucose detection (see section 'Polymer Functionalization') [43]. These functionalized nanoelectrodes exhibited maximal sensitivities of 36 μA cm^{-2} mM^{-1} for 6 μm high nanopillars, the highest glucose sensitivity of gold nanopillar devices reported thus far. Moreover, the sensitivity was about 12 times higher than the value Anandan et al. previously reported for nanopillars of the same geometry functionalized with MPA and GOx [50].

Nonenzymatic glucose detection was recently presented for gold nanopillars of 70 nm diameter [49]. This study compared the voltammetric detection via cyclic voltammetry (CV) and differential pulse voltammetry with amperometric glucose sensing. Voltammetry yielded a sensitivity of 41.9 μA mM^{-1} cm^{-2} with a detection limit below 30 μM and a linear detection range up to 20 mM. For amperometric detection a linear correlation with the glucose concentration was found in the range of 1–10 mM. The sensitivity in this regime was very high at 309.0 μA mM^{-1} cm^{-2}, where a detection limit of 50 μM glucose was reported. Au nanopillar electrodes also showed good long-term stability, being utilized for up to two months with storage at ambient conditions. For practical applications, and because of the increased sensitivity, the use of amperometric gold nanopillar sensors was positively recommended in this study.

Gold nanopillar biosensors have also been applied as biotin detectors by anchoring an avidin functionalization onto MUA [144]. This setup was used for voltammetric detection and electrical impedance spectroscopy (EIS) of biotin diluted in phosphate-buffered saline (PBS) solution. The detection range for this avidin-based sensor was 1–50 ng/ml, while in CV experiments the sensitivity ranged from 0.5 to 4.2 $(mF\ ng)^{-1}$ ml mm^{-2}, corresponding to a 27–221 times increase over planar gold sensors. The sensitivity in EIS measurements was between 159 and 845 $\Omega(ng)^{-1}$ ml mm^{-2}, an increase by a factor of 10.8–57.6 compared to planar gold electrodes. Overall, EIS measurements were more sensitive than CV in discriminating small changes due to surface adsorption of different molecules.

Recently, microelectrodes were modified with gold nanopillars (60 nm diameter, 300–400 nm height) to record action potentials from HL-1 cells [46]. The cells were cultivated on arrays of 64 pillar-modified electrodes with a fibronectin coating and diameters ranging from 8 to 20 μm. Due to the large surface area, the impedance of the nanopillar electrodes was strongly decreased compared to smooth electrodes. As a result, increased action potentials were measured yielding maximal peak-to-peak amplitudes of up to 1.5 mV with RMS noise levels of 6–7 μV. Compared to planar gold microelectrodes, the pillar electrodes yielded up to 100 % greater signal amplitudes. Nick et al. modified microelectrodes with even larger gold nanopillars, which were between 4 and 22.5 μm high. In cell culture experiments with neurons these sensors yielded signal amplitudes which were up to ten times higher than with planar gold electrodes [156]. In the future nanopillar electrodes with tailored geometries and larger heights in particular might also enable the recording of intracellular signals, similar to the concept of gold microspines as introduced by Hai et al. [8].

Table 11.5 Performance characteristics of plasmonic applications with gold nanopillars

Plasmonic device	Application	Performance characteristics	References
Polymer nanopillars with gold caps, SAM coating, and goat IgG	Plasmonic biosensor for human IgG	Detection limit: 1 ng/ml (corresponds to 6.7 pM)	Saito et al. [72]
Solid gold nanopillars with CdSe-ZnS quantum dots on protein linkers	Fluorescence applications	Fifteen-fold increase in surface-plasmon-enhanced fluorescence	Zin et al. [25]
Solid gold nanopillars with Fe_2O_3 coating	Electrodes for catalytic water splitting	50 % increase in photocurrent density compared to planar electrodes	Gao et al. [71]
Ag/Au nanodisks on top of HSQ nanoposts	High-resolution printing and optical data storage	Printing at the limit of visible-light imaging with a resolution of 100,000 dpi	Kumar et al. [151]
Solid gold nanopillar arrays	Plasmonic nano-tweezer	Stable trapping of polystyrene beads with 110 nm diameter	Wang et al. [78]
Gold-capped silicon nanopillars	SERS-based biochemical sensors	Enhancement factors of up to 1.2×10^8	Caldwell et al. [152]
Poly(3-hexylthiphene) and [6,6]-phenyl C61 butyric acid methyl ester with gold nanopillars	Organic photovoltaic device	Peak enhancement of 60 % at a wavelength of 675 nm	Tsai et al. [26]
AAO/Au composite	Plasmonic biosensing with streptavidin-biotin	Detection limit of 300nM for biotin, corresponding to two orders of magnitude better than SPR sensors with continuous films	Kabashin et al. [155]
Solid gold nanopillar array	Optical detection of protein adsorption	Detection of lysozyme and bovine serum albumine: sensitivity of 246 ± 12 nm wavelength shift per refractive index unit	Pallarola et al. [157]

Gold Nanopillars in Plasmonic Devices

Gold nanopillars that have been implemented into plasmonic sensing devices also contribute to improved sensing performance (see Table 11.5). Pallarola et al. fabricated electrically active gold nanopillar arrays from PC membranes, which they used for the optical detection of protein adsorption. With nanopillars of approximately 100 nm diameter and 1.9 μm in height they could influence the adsorption kinetics of lysozyme and bovine serum albumine by electrochemical modulation [157]. Recently, polymer nanopillars from COP (40 and 65 nm in diameter) were modified with gold caps to create plasmonic sensors for human IgG. The gold caps were coated with a 10-carboxyl-1-decanethiol SAM, followed by a functionalization with goat antihuman IgG [72]. For the optical absorbance of the anti-IgG-immobilized Au-capped nanopillars, a linear detection range up to

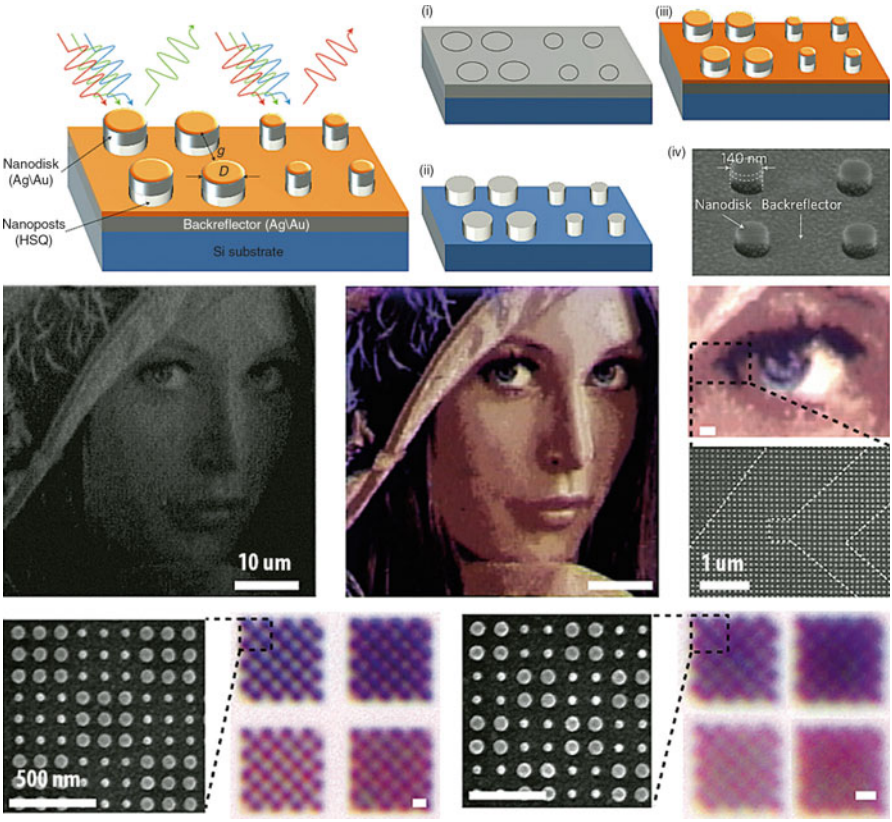

Fig. 11.10 Geometry-controlled, gold-coated HSQ/aluminum nanopillars are used to produce color images with a resolution of up to 100,000 dpi (Reproduced from [151], copyright 2012 Nature Publishing Group)

100 µg/ml was found. These gold nanopillar sensors displayed a detection limit of only 1 ng/ml, which corresponds to 6.7 pM IgG. In a previous study on plasmonic IgG sensors with horizontal gold nanorods 50 nm long and 15 nm in diameter, the detection limit was found to be only about 1 nM [150]. Thus, vertical gold nanostructures – even when only capped by gold – exhibit a superior binding capacity and sensitivity compared to lying nanorods.

Gold nanopillars were recently modified with CdSe-ZnS quantum dots for fluorescence applications by using a molecular biotin-streptavidin linker [25]. This arrangement yielded an increase in surface-plasmon-enhanced photoluminescence; up to a factor of 15 was achieved for 50 nm tall nanopillar arrays with 100 nm diameter and a grating constant of 100 nm. The fluorescence increase was also found to depend on the length of the molecular spacer between the quantum dots and pillar tips, where 16 nm was the optimum spacer length in this study. The biotin-streptavidin affinity model was also used by Kabashin et al. to demonstrate

plasmonic biosensing with gold nanopillars embedded in AAO templates [155]. The AAO/Au metamaterial yielded a detection limit of 300 nM for biotin and was shown to be two orders of magnitude better than conventional SPR sensors with continous films.

By coating gold nanopillars with Fe_2O_3, thin-film electrodes were designed that could be used for plasmon-enhanced photocatalytic water splitting [71]. With an oxide layer of 50 nm, the photocurrent density was enhanced by 50 % compared to planar electrodes. This enhancement was attributed to the increased optical absorption, which originated from surface-plasmon resonances and photonic-mode light trapping in the nanostructures.

Gold coating of hydrogen silsesquioxane (HSQ)/aluminum nanopillars formed on a backside reflecting material such as aluminum can be applied to the creation of some rather spectacular color images [151]. As shown in Fig. 11.10, the reproduction of color spectra is achieved by selective tuning of the plasmonically active nanopillar dimensions to form pixels of the desired color. Such a methodology has possible applications in the creation of imprinted color features on various media or for security purposes. Nakamoto et al. also fabricated nanopillar-hole structures for plasmonic nanogap devices [70], while linear arrays of gold nanopillars have been demonstrated to act as plasmonic waveguides through coupling of plasmons [28]. Wang et al. utilized plasmon trapping with gold nanopillars to form optical tweezers for the manipulation of small particles. With this design they were able to trap and rotate polystyrene spheres with diameters down to 110 nm [48, 78]. Gold-capped silicon nanopillar arrays were fabricated by Caldwell et al. for use in SERS-based chemical sensors, and thiophenol SAM showed an enhancement factor of over eight orders of magnitude greater than the bare-structured surface [152]. Furthermore, gold nanopillar arrays have recently been used in prototype organic photovoltaic devices to improve their performance. The novel solar cells exhibited an increased quantum efficiency between 640 and 720 nm compared to devices without nanopillars; at 675 nm the peak enhancement was around 60 % [26].

References

1. Eustis S, El-Sayed MA (2006) Why gold nanoparticles are more precious than pretty gold: noble metal surface plasmon resonance and its enhancement of the radiative and nonradiative properties of nanocrystals of different shapes. Chem Soc Rev 35(3):209–217
2. Duan GT et al (2006) Electrochemically induced flowerlike gold nanoarchitectures and their strong surface-enhanced Raman scattering effect. Appl Phys Lett 89(21):211905–3
3. Murphy CJ et al (2005) Anisotropic metal nanoparticles: synthesis, assembly, and optical applications. J Phys Chem B 109(29):13857–13870
4. Kim F et al (2008) Chemical synthesis of gold nanowires in acidic solutions. J Am Chem Soc 130(44):14442–14443
5. Seker E et al (2010) The fabrication of low-impedance nanoporous gold multiple-electrode arrays for neural electrophysiology studies. Nanotechnology 21(12):125504
6. Nishio K, Masuda H (2011) Anodization of gold in oxalate solution to form a nanoporous black film. Angew Chem Int Ed 50(7):1603–1607

7. Kim JH et al (2010) Surface-modified microelectrode array with flake nanostructure for neural recording and stimulation. Nanotechnology 21(8):85303
8. Hai A, Shappir J, Spira ME (2010) In-cell recordings by extracellular microelectrodes. Nat Methods 7(3):200–202
9. Panaitov G et al (2011) Fabrication of gold micro-spine structures for improvement of cell/device adhesion. Microelectron Eng 88(8):1840–1844
10. Choi MK et al (2011) Simple fabrication of asymmetric high-aspect-ratio polymer nanopillars by reusable AAO templates. Langmuir 27(6):2132–2137
11. Schmidt MS, Hübner J, Boisen A (2012) Large area fabrication of leaning silicon nanopillars for surface enhanced raman spectroscopy. Adv Mater 24(10):OP11–OP18
12. Xie C et al (2010) Noninvasive neuron pinning with nanopillar arrays. Nano Lett 10(10):4020–4024
13. Xie C et al (2011) Vertical nanopillars for highly localized fluorescence imaging. Proc Natl Acad Sci USA 108(10):3894–3899
14. Lin A et al (2012) Extracting transport parameters in GaAs nanopillars grown by selective-area epitaxy. Nanotechnology 23(10):105701
15. Jang D et al (2012) Deformation mechanisms in nanotwinned metal nanopillars. Nat Nanotechnol 7(9):594–601
16. Anandan V, Rao YL, Zhang G (2005) Nanopillar arrays with superior mechanical strength and optimal spacing for high sensitivity biosensors. NSTI-Nanotech 3
17. Yang M et al (2006) Platinum nanowire nanoelectrode array for the fabrication of biosensors. Biomaterials 27(35):5944–5950
18. Vlad A et al (2008) Nanowire-decorated microscale metallic electrodes. Small 4(5):557–560
19. Tian JH et al (2011) Fabrication of high density metallic nanowires and nanotubes for cell culture studies. Microelectron Eng 88(8):1702–1706
20. Buzzi S et al (2008) Metal direct nanoimprinting for photonics. Microelectron Eng 85(2):419–424
21. Ulman A (1996) Formation and structure of self-assembled monolayers. Chem Rev 96(4):1533–1554
22. Hulteen JC, Martin CR (1997) A general template-based method for the preparation of nanomaterials. J Mater Chem 7(7):1075–1087
23. Foss CA et al (1992) Optical-properties of composite membranes containing arrays of nanoscopic gold cylinders. J Phys Chem 96(19):7497–7499
24. Greer JR, Nix WD (2005) Size dependence of mechanical properties of gold at the sub-micron scale. Appl Phys A 80(8):1625–1629
25. Zin MT et al (2009) Surface-plasmon-enhanced fluorescence from periodic quantum dot arrays through distance control using biomolecular linkers. Nanotechnology 20(1):015305
26. Tsai SJ et al (2010) Effect of gold nanopillar arrays on the absorption spectrum of a bulk heterojunction organic solar cell. Opt Express 18(Suppl 4):A528–A535
27. Cetin AE et al (2011) Monopole antenna arrays for optical trapping, spectroscopy, and sensing. Appl Phys Lett 98(11):111110–111113
28. Dhawan A et al (2009) Fabrication of nanodot plasmonic waveguide structures using FIB milling and electron beam-induced deposition. Scanning 31(4):139–146
29. Possin GE (1970) A method for forming very small diameter wires. Rev Sci Instrum 41(5):1684640–1684642
30. Martin CR (1996) Membrane-based synthesis of nanomaterials. Chem Mater 8(8):1739–1746
31. Huczko A (2000) Template-based synthesis of nanomaterials. Appl Phys A Mater Sci Process 70(4):365–376
32. Ghicov A, Schmuki P (2009) Self-ordering electrochemistry: a review on growth and functionality of TiO_2 nanotubes and other self-aligned MO*x* structures. Chem Commun 20(20):2791–2808
33. Diggle JW, Downie TC, Goulding CW (1969) Anodic oxide films on aluminum. Chem Rev 69(3):365–405

34. Sulka GD (2008) Highly ordered anodic porous alumina formation by self-organized anodizing. In: Eftekhari A (ed) Nanostructured materials in electrochemistry. Wiley, Weinheim, pp 1–116
35. Fischer BE, Spohr R (1983) Production and use of nuclear tracks – imprinting structure on solids. Rev Mod Phys 55(4):907–948
36. Apel P (2001) Track etching technique in membrane technology. Radiat Meas 34(1–6):559–566
37. Brumlik CJ, Menon VP, Martin CR (1994) Template synthesis of metal microtubule ensembles utilizing chemical, electrochemical, and vacuum deposition techniques. J Mater Res 9(5):1174–1183
38. Brumlik CJ, Martin CR (1991) Template synthesis of metal microtubules. J Am Chem Soc 113(8):3174–3175
39. Martin CR (1991) Template synthesis of polymeric and metal microtubules. Adv Mater 3(9):457–459
40. Evans P et al (2006) Growth and properties of gold and nickel nanorods in thin film alumina. Nanotechnology 17(23):5746
41. Anandan V, Gangadharan R, Zhang G (2009) Role of SAM chain length in enhancing the sensitivity of nanopillar modified electrodes for glucose detection. Sensors (Basel) 9(3):1295–1305
42. Forrer P et al (2000) Electrochemical preparation and surface properties of gold nanowire arrays formed by the template technique. J Appl Electrochem 30(5):533–541
43. Gangadharan R, Anandan V, Zhang G (2008) Optimizing the functionalization process for nanopillar enhanced electrodes with GOx/PPY for glucose detection. Nanotechnology 19(39):395501
44. Greer JR, Oliver WC, Nix WD (2005) Size dependence of mechanical properties of gold at the micron scale in the absence of strain gradients. Acta Mater 53(6):1821–1830
45. Nagel PM et al (2012) Surface plasmon assisted electron acceleration in photoemission from gold nanopillars. Chem Phys 414:106–111
46. Brüggemann D et al (2011) Nanostructured gold microelectrodes for extracellular recording from electrogenic cells. Nanotechnology 22(26):265104
47. Brüggemann D et al (2012) Adhesion and survival of electrogenic cells on gold nanopillar array electrodes. Int J Nano Biomater 4(2):108–127
48. Wang K, Crozier KB (2012) Plasmonic trapping with a gold nanopillar. Chemphyschem 13(11):2639–2648
49. Cherevko S, Chung CH (2009) Gold nanowire array electrode for non-enzymatic voltammetric and amperometric glucose detection. Sensor Actuator B Chem 142(1):216–223
50. Anandan V et al (2007) Role of reaction kinetics and mass transport in glucose sensing with nanopillar array electrodes. J Biol Eng 1:5
51. Shin C, Shin W, Hong H-G (2007) Electrochemical fabrication and electrocatalytic characteristics studies of gold nanopillar array electrode (AuNPE) for development of a novel electrochemical sensor. Electrochim Acta 53(2):720–728
52. Menon VP, Martin CR (1995) Fabrication and evaluation of nanoelectrode ensembles. Anal Chem 67(13):1920–1928
53. Demoustier-Champagne S, Delvaux M (2001) Preparation of polymeric and metallic nanostructures using a template-based deposition method. Mater Sci Eng C 15(1–2):269–271
54. Wirtz M, Martin CR (2003) Template-fabricated gold nanowires and nanotubes. Adv Mater 15(5):455–458
55. Delvaux M, Demoustier-Champagne S, Walcarius A (2004) Flow injection amperometric detection at enzyme-modified gold nanoelectrodes. Electroanalysis 16(3):190–198
56. Delvaux M, Walcarius A, Demoustier-Champagne S (2004) Electrocatalytic H_2O_2 amperometric detection using gold nanotube electrode ensembles. Anal Chim Acta 525(2):221–230

57. Krishnamoorthy K, Zoski CG (2005) Fabrication of 3D gold nanoelectrode ensembles by chemical etching. Anal Chem 77(15):5068–5071
58. Moretto LM, Pepe N, Ugo P (2004) Voltammetry of redox analytes at trace concentrations with nanoelectrode ensembles. Talanta 62(5):1055–1060
59. Brunetti B et al (2000) Electrochemistry of phenothiazine and methylviologen biosensor electron-transfer mediators at nanoelectrode ensembles. J Electroanal Chem 491(1–2):166–174
60. Anandan V, Rao YL, Zhang G (2006) Nanopillar array structures for enhancing biosensing performance. Int J Nanomedicine 1(1):73–79
61. Reyntjens S, Puers R (2001) A review of focused ion beam applications in microsystem technology. J Micromech Microeng 11:287–300
62. Volkert CA, Lilleodden ET (2006) Size effects in the deformation of sub-micron Au columns. Philos Mag 86(33–35):5567–5579
63. Dietiker M et al (2011) Deformation behavior of gold nano-pillars prepared by nanoimprinting and focused ion-beam milling. Acta Mater 59(5):2180–2192
64. Lee SW, Han SM, Nix WD (2009) Uniaxial compression of fcc Au nanopillars on an MgO substrate: the effects of prestraining and annealing. Acta Mater 57(15):4404–4415
65. Lancon F et al (2010) Superglide at an internal incommensurate boundary. Nano Lett 10(2):695–700
66. Greer JR, Nix WD (2006) Nanoscale gold pillars strengthened through dislocation starvation. Phys Rev B 73(24):245410
67. Lehrer C et al (2000) Defects and gallium – contamination during focused ion beam micro machining. In: IEEE conference proceedings: ion implantation technology, 2000. Conference on Ion Implantation Technology, Alpbach, 2000. pp 695–698
68. Ahn SH, Guo LJ (2008) High-speed roll-to-roll nanoimprint lithography on flexible plastic substrates. Adv Mater 20:2044–2049
69. Liang C-C et al (2011) Plasmonic metallic nanostructures by direct nanoimprinting of gold nanoparticles. Opt Express 19(5):4768–4776
70. Nakamoto K, Kurita R, Niwa O (2011) Arrays of metallic nanopillars in holes for plasmonic devices. In: 15th international conference on miniaturized systems for chemistry and life sciences, Seattle
71. Gao H et al (2012) Plasmon-enhanced photocatalytic activity of iron oxide on gold nanopillars. ACS Nano 6(1):234–240
72. Saito M et al (2012) Novel gold-capped nanopillars imprinted on a polymer film for highly sensitive plasmonic biosensing. Anal Chem 84(13):5494–5500
73. Kubo W, Fujikawa S (2010) Au double nanopillars with nanogap for plasmonic sensor. Nano Lett 11(1):8–15
74. Wolfrum B et al (2006) Fabrication of large-scale patterned gold-nanopillar arrays on a silicon substrate using imprinted porous alumina templates. Small 2(11):1256–1260
75. Mátéfi-Tempfli S et al (2009) Nanowires and nanostructures fabrication using template methods: a step forward to real devices combining electrochemical synthesis with lithographic techniques. J Mater Sci Mater Electron 20(1):249–254
76. Weber D et al (2011) Large-scale patterning of gold nanopillars in a porous anodic alumina template by replicating gold structures on a titanium barrier. J Nanosci Nanotechnol 11(2):1293–1296
77. Einsle JF et al (2012) Directed self-assembly of nanorod networks: bringing the top down to the bottom up. Nanotechnology 23(50):505302
78. Wang K et al (2011) Trapping and rotating nanoparticles using a plasmonic nano-tweezer with an integrated heat sink. Nat Commun 2:469
79. Zepeda-Ruiz LA et al (2007) Mechanical response of freestanding Au nanopillars under compression. Appl Phys Lett 91(10):101907-3
80. Rabkin E, Srolovitz DJ (2007) Onset of plasticity in gold nanopillar compression. Nano Lett 7:101–107

81. Ye JC et al (2010) Extraction of bulk metallic-glass yield strengths using tapered micropillars in micro-compression experiments. Intermetallics 18(3):385–393
82. Lin JS, Ju SP, Lee WJ (2005) Mechanical behavior of gold nanowires with a multishell helical structure. Phys Rev B 72(8):085448
83. Afanasyev KA, Sansoz F (2007) Strengthening in gold nanopillars with nanoscale twins. Nano Lett 7(7):2056–2062
84. Rabkin E, Srolovitz DJ (2006) Onset of plasticity in gold nanopillar compression. Nano Lett 7(1):101–107
85. Diao J et al (2006) Atomistic simulations of the yielding of gold nanowires. Acta Mater 54(3):643–653
86. Diao JK, Gall K, Dunn ML (2004) Yield strength asymmetry in metal nanowires. Nano Lett 4(10):1863–1867
87. Weinberger CR, Cai W (2008) Surface-controlled dislocation multiplication in metal micropillars. Proc Natl Acad Sci USA 105(38):14304–14307
88. Wurtz GA et al (2011) Designed ultrafast optical nonlinearity in a plasmonic nanorod metamaterial enhanced by nonlocality. Nat NanoTechnol 6(2):107–111
89. Pollard RJ et al (2009) Optical nonlocalities and additional waves in epsilon-near-zero metamaterials. Phys Rev Lett 102(12):127405
90. Spatz JP, Geiger B (2007) Molecular engineering of cellular environments: cell adhesion to nano digital surfaces. In: Yu-Li W, Dennis ED (eds) Methods in cell biology. Academic, New York, pp 89–111
91. Curtis ASG et al (2001) Substratum nanotopography and the adhesion of biological cells. Are symmetry or regularity of nanotopography important? Biophys Chem 94(3):275–283
92. Haq F et al (2007) Neurite development in PC12 cells cultured on nanopillars and nanopores with sizes comparable with filopodia. Int J Nanomedicine 2(1):107–115
93. Wightman RM (1981) Microvoltammetric electrodes. Anal Chem 53(9):1125A–1134A
94. Wightman RM (2006) Probing cellular chemistry in biological systems with microelectrodes. Science 311(5767):1570–1574
95. Cans A-S, Ewing AG (2011) Highlights of 20 years of electrochemical measurements of exocytosis at cells and artificial cells. J Solid State Electr 15(7–8):1437–1450
96. Smith C, White H (1993) Theory of the voltammetric response of electrodes of submicron dimensions – violation of electroneutrality in the presence of excess supporting electrolyte. Anal Chem 65(23):3343–3353
97. Bond AM, Oldham KB, Zoski CG (1989) Steady-state voltammetry. Anal Chim Acta 216:177–230
98. Conyers JL, White HS (2000) Electrochemical characterization of electrodes with submicrometer dimensions. Anal Chem 72(18):4441–4446
99. Amatore C, Maisonhaute E (2005) When voltammetry reaches nanoseconds. Anal Chem 77(15):303A–311A
100. Baltes N et al (2004) Imaging concentration profiles of redox-active species with nanometric amperometric probes: effect of natural convection on transport at microdisk electrodes. Angew Chem Int Ed 43(11):1431–1435
101. Wehmeyer KR, Deakin MR, Wightman RM (1985) Electroanalytical properties of band electrodes of submicrometer width. Anal Chem 57(9):1913–1916
102. Bond AM, Henderson TLE, Thormann W (1986) Theory and experimental characterization of linear gold microelectrodes with submicrometer thickness. J Phys Chem 90(13):2911–2917
103. Morris RB, Franta DJ, White HS (1987) Electrochemistry at platinum bane electrodes of width approaching molecular dimensions: breakdown of transport equations at very small electrodes. J Phys Chem 91(13):3559–3564
104. Arrigan DWM (2004) Nanoelectrodes, nanoelectrode arrays and their applications. Analyst 129(12):1157–1165

105. Dudin PV et al (2011) Electrochemistry at nanoscale electrodes: individual single-walled carbon nanotubes (SWNTs) and SWNT-templated metal nanowires. ACS Nano 5(12):10017–10025
106. Rassaei L, Singh PS, Lemay SG (2011) Lithography-based nanoelectrochemistry. Anal Chem 83(11):3974–3980
107. Cox JT, Zhang B (2012) Nanoelectrodes: recent advances and new directions. In: Cooks RG, Yeung ES (eds) Annual review of analytical chemistry, vol 5. Annu Rev, Palo Alto, pp 253–272
108. Oja SM, Wood M, Zhang B (2013) Nanoscale electrochemistry. Anal Chem 85(2):473–486
109. Sanderson DG, Anderson LB (1985) Filar electrodes: steady-state currents and spectroelectrochemistry at twin interdigitated electrodes. Anal Chem 57(12):2388–2393
110. Bard AJ et al (1989) Scanning electrochemical microscopy. Introduction and principles. Anal Chem 61(2):132–138
111. Macpherson JV, Unwin PR (2000) Combined scanning electrochemical-atomic force microscopy. Anal Chem 72(2):276–285
112. Sun P, Laforge FO, Mirkin MV (2007) Scanning electrochemical microscopy in the 21st century. Phys Chem Chem Phys 9(7):802–823
113. Edwards MA et al (2006) Scanning electrochemical microscopy: principles and applications to biophysical systems. Physiol Meas 27(12):R63–R108
114. Amemiya S et al (2008) Scanning electrochemical microscopy. In: Annual review of analytical chemistry. Annal Reviews, Palo Alto, pp 95–131
115. Schulte A, Nebel M, Schuhmann W (2010) Scanning electrochemical microscopy in neuroscience. Annu Rev Anal Chem 3(1):299–318
116. Takahashi Y et al (2012) Topographical and electrochemical nanoscale imaging of living cells using voltage-switching mode scanning electrochemical microscopy. Proc Natl Acad Sci 109(29):11540–11545
117. Fan F-RF, Bard AJ (1995) Electrochemical detection of single molecules. Science 267(5199):871–874
118. Fan F-RF, Kwak J, Bard AJ (1996) Single molecule electrochemistry. J Am Chem Soc 118(40):9669–9675
119. Sun P, Mirkin MV (2008) Electrochemistry of individual molecules in zeptoliter volumes. J Am Chem Soc 130(26):8241–8250
120. Zevenbergen MA et al (2011) Stochastic sensing of single molecules in a nanofluidic electrochemical device. Nano Lett 11(7):2881–2886
121. Singh PS et al (2012) Stochasticity in single-molecule nanoelectrochemistry: origins, consequences, and solutions. ACS Nano 6(11):9662–9671
122. Lemay SG et al (2012) Single-molecule electrochemistry: present status and outlook. Acc Chem Res 46(2):369–377
123. Kätelhön E, Wolfrum B (2012) On-chip redox cycling techniques for electrochemical detection. Rev Anal Chem 31(1):7–14
124. Hulteen JC, Menon VP, Martin CR (1996) Template preparation of nanoelectrode ensembles – achieving the "pure-radial" electrochemical-response limiting case. J Chem Soc Faraday Trans 92(20):4029–4032
125. Martin CR, Mitchell DT (1999) Template-synthesized nanomaterials in electrochemistry. In: Bard AJ, Rubinstein I (eds) Electroanalytical chemistry, vol 21. Marcel Dekker, New York, pp 1–74
126. Jeoung E et al (2001) Fabrication and characterization of nanoelectrode arrays formed via block copolymer self-assembly. Langmuir 17(21):6396–6398
127. Li J et al (2002) Novel three-dimensional electrodes: electrochemical properties of carbon nanotube ensembles. J Phys Chem B 106(36):9299–9305
128. Schmid G (2002) Materials in nanoporous alumina. J Mater Chem 12(5):1231–1238

129. Cheng WL, Dong SJ, Wang EK (2002) Gold nanoparticles as fine tuners of electrochemical properties of the electrode/solution interface. Langmuir 18(25):9947–9952
130. Ugo P, Moretto LM, Vezza F (2002) Ionomer-coated electrodes and nanoelectrode ensembles as electrochemical environmental sensors: recent advances and prospects. Chemphyschem 3(11):917–925
131. Yamada K, Gasparac R, Martin CR (2004) Electrochemical and transport properties of templated gold/polypyrrole-composite microtube membranes. J Electrochem Soc 151(1): E14–E19
132. Lin YH et al (2004) Glucose biosensors based on carbon nanotube nanoelectrode ensembles. Nano Lett 4(2):191–195
133. Koehne J et al (2004) The fabrication and electrochemical characterization of carbon nanotube nanoelectrode arrays. J Mater Chem 14(4):676–684
134. LaFratta CN, Walt DR (2008) Very high density sensing arrays. Chem Rev 108(2):614–637
135. Ugo P et al (2010) Diffusion regimes at nanoelectrode ensembles in different ionic liquids. Electrochim Acta 55(8):2865–2872
136. Schröper F et al (2008) Analyzing the electroactive surface of gold nanopillars by electrochemical methods for electrode miniaturization. Electrochim Acta 53(21):6265–6272
137. Sanetra N et al (2011) Low impedance surface coatings via nanopillars and conductive polymers. Physica Status Solidi A 208(6):1284–1289
138. Zhou H-B et al (2009) Integration of Au nanorods with flexible thin-film microelectrode arrays for improved neural interfaces. J Microelectromech Syst 18(1):88–96
139. Hai A et al (2009) Spine-shaped gold protrusions improve the adherence and electrical coupling of neurons with the surface of micro-electronic devices. J R Soc Interface 6(41):1153–1165
140. Hai A et al (2009) Changing gears from chemical adhesion of cells to flat substrata toward engulfment of micro-protrusions by active mechanisms. J Neural Eng 6(6):066009
141. Nam Y (2012) Material considerations for in vitro neural interface technology. MRS Bulletin 37(6):566–572
142. Spira ME, Hai A (2013) Multi-electrode array technologies for neuroscience and cardiology. Nat Nanotechnol 8(2):83–94
143. Delvaux M, Demoustier-Champagne S (2003) Immobilisation of glucose oxidase within metallic nanotubes arrays for application to enzyme biosensors. Biosens Bioelectron 18(7):943–951
144. Lee S-J, Anandan V, Zhang G (2008) Electrochemical fabrication and evaluation of highly sensitive nanorod-modified electrodes for a biotin/avidin system. Biosens Bioelectron 23(7):1117–1124
145. Wang X-Y et al (2004) Direct electrochemical fabrication of metallic nanopillar array on Au electrode surface by the template technique. Chem Lett 33(8):982–983
146. Wang Z, Su YK, Li HL (2002) AFM study of gold nanowire array electrodeposited within anodic aluminum oxide template. Appl Phys A 74(4):563–565
147. Brumlik CJ, Martin CR, Tokuda K (1992) Microhole array electrodes based on microporous alumina membranes. Anal Chem 64(10):1201–1203
148. Sapp SA, Mitchell DT, Martin CR (1999) Using template-synthesized micro- and nanowires as building blocks for self-assembly of supramolecular architectures. Chem Mater 11(5):1183–1185
149. Yu S et al (2003) Nano wheat fields prepared by plasma-etching gold nanowire-containing membranes. Nano Lett 3(6):815–818
150. Mayer KM et al (2008) A label-free immunoassay based upon localized surface plasmon resonance of gold nanorods. ACS Nano 2(4):687–692
151. Kumar K et al (2012) Printing colour at the optical diffraction limit. Nat Nanotechnol 7(9):557–561

152. Caldwell JD et al (2011) Plasmonic nanopillar arrays for large-area, high-enhancement surface-enhanced Raman scattering sensors. ACS Nano 5(5):4046–4055
153. Schneckenburger M et al (2012) Cross-sectional characterization of electrodeposited, monocrystalline Au nanowires in parallel arrangement. Small 8(22):3396–3399
154. Wang H-W et al (2006) Standing [111] gold nanotube to nanorod arrays via template growth. Nanotechnology 17(10):2689–2694
155. Kabashin AV et al (2009) Plasmonic nanorod metamaterials for biosensing. Nat Mater 8 (11):867–871
156. Nick C et al. (2013) High aspect ratio gold nanopillars on microelectrodes for neural interfaces. Microsyst Technol
157. Pallarola D et al. (2013) Real-time monitoring of electrochemical controlled protein adsorption by a plasmonic nanowire based sensor. Chem Comm 49:8326–8328